ERC-R-97-017

FINAL REPORT

DESIGN STUDY - ROCKET BASED MHD GENERATOR

NASA Purchase Order No. H-13047D

Submitted to:
National Aeronautics and Space Administration
George C. Marshall Space Flight Center
Marshall Space Flight Center, AL 35812

Submitted by:
ERC Incorporated
Tullahoma Operations Office
1940 Elk River Dam Road
Tullahoma, TN 37388

May 1997

ERC
INCORPORATED

1940 Elk River Dam Rd.
P.O. Box 417
Tullahoma, TN 37388
Tel: 615/455.9915
Fax: 615/454.2042

TABLE OF CONTENTS

Section	Page
Table of Contents	i
List of Figures	ii
Summary	iv
1. Introduction	1
2. Lox/RP Rocket Motor Thermo/Plasmadynamic Characterization	1
2.1. Seeding	3
2.2. Generator Entry Point Selection	4
3. Design Analysis	5
3.1. Magnet Constraint	8
3.2. Other Constraints	9
3.3. Generator Performance	10
4. Conceptual MHD Channel Design	25
5. Rocket Based MHD Accelerator	30
6. Conclusions and Recommendations	33
7. References	35
Appendix A - Review of Russian Works by Valentin Bityurin	37

LIST OF FIGURES

Figure **Page**

1: Sub-Scale Rocket Motor of MSFC (SNTL - D - 500 - 1000, Liquid Fuel) 2

2: Plasma Conductivity Variation with Seeding Percentage of Potassium and Cesium at Various Combustion Conditions of LOx/RP Rocket Motors 4

3: Power Density Parameter Distribution along 300 psi LOx/RP Rocket Nozzle with Different Potassium Seeding Percentages 6

4: Power Density Parameter Distribution along 300 psi LOx/RP Rocket Nozzle with Different Cesium Seeding Percentages 6

5: Loading Configuration of a Faraday Generator with Segmented Electrodes and a Hall Generator 7

6: Normalized Magnetic Flux Density Distribution of ECF Magnet 9

7: Calculated Flow and Electrical Parameter Distributions for the Constant Mach Number Faraday Generator. RP1 + O2 + KOH, K(wt.%) = 3.74, $P_{comb.}$ = 300 psi, B = 1.5 T, Mass Flow = 0.228 Kg/s, $A_{MHD.inlet}/A_{throat}$ = 8., Channel Length = 20 inches. (Equilibrium Flow Assumption) 13

8: Geometry of the Designed MHD Channel 14

9: Calculated Flow and Electrical Parameter Distributions for the Designed 4° Half Wall Angle Faraday Generator. RP1 + O2 + KOH, K(wt.%) = 3.74, $P_{comb.}$ = 300 psi, B = 1.5 T, Mass Flow = 0.228 Kg/s, $A_{MHD.inlet}/A_{throat}$ = 9.82, Channel Length = 20 inches. (Equilibrium Flow Assumption) 16

10: Calculated Flow and Electrical Parameter Distributions for the Designed 4° Half Wall Angle Faraday Generator. RP1 + O2 + KOH, K(wt.%) = 3.74, $P_{comb.}$ = 300 psi, B = 1.5 T, Mass Flow = 0.228 Kg/s, $A_{MHD.inlet}/A_{throat}$ = 9.82, Channel Length = 20 inches. (Frozen Flow Assumption) 17

11: Loading Conditions for the Designed 4° Half Wall Angle Faraday Generator Using Potassium Seed. (Solid Lines: Equilibrium Flow, Dashed Lines: Frozen Flow) 18

12: Relation between Thrust, Electrical Power, and Total Pressure Loss in the Channel of the Designed Rocket Driven MHD Generator Using Potassium Seed. (Solid Lines: Equilibrium Flow, Dashed Lines: Frozen Flow) 19

13: Calculated Flow and Electrical Parameter Distributions for the Designed 4° Half Wall Angle Faraday Generator. RP1 + O2 + CsOH, Cs(wt.%) = 9.66, $P_{comb.}$ = 300 psi, B = 1.5 T, Mass Flow = 0.235 Kg/s, $A_{MHD.inlet}/A_{throat}$ = 9.82, Channel Length = 20 inches (Equilibrium Flow Assumption) 21

Figure **Page**

14: Calculated Flow and Electrical Parameter Distributions for the Designed 4° Half Wall Angle Faraday Generator. RP1 + O2 + CsOH, Cs(wt.%) = 9.66, $P_{comb.}$ = 300 psi, B = 1.5 T, Mass Flow = 0.235 Kg/s, $A_{MHD.inlet}/A_{throat}$ = 9.82, Channel Length = 20 inches (Frozen Flow Assumption). 22

15: Loading Conditions for the Designed 4° Half Wall Angle Faraday Generator Using Cesium Seed. (Solid Lines: Equilibrium Flow, Dashed Lines: Frozen Flow) 23

16: Relation between Thrust, Electrical Power, and Total Pressure Loss in the Channel of the Designed Rocket Driven MHD Generator Using Cesium Seed. (Solid Lines: Equilibrium Flow, Dashed Lines: Frozen Flow) 24

17: Conceptual Design of Electrode Wall Assembly for Faraday Channel 26

18: Conceptual Design of Insulating Sidewall Assembly for Faraday Channel 27

19: Conceptual Design of Heat Sink Faraday Channel Assembly 28

20: Schematic of Small-Scale Rocket Based MHD System 29

21: Schematic of Testing Confiduration for Small-Scale Rocket Based MHD System 29

22: Performance Diagram for Ideal Faraday MHD Accelerator with a Conductivity of 30 Siemens/m (Solid Lines: uB = 15 kV/m, Dashed Lines: uB = 10 kV/m, Dash-Dotted Lines: uB = 5 kV/m) 32

23: Comparison of Performance for Ideal Faraday Accelerator with Different Conductivities 33

SUMMARY

This Final Report represents the final contract deliverable for NASA MSFC Purchase Order No. H-13047D, entitled:

Design Study - Rocket Based MHD Generator

The Final Report addresses the technical feasibility and design of a rocket based MHD generator using a sub-scale LOx/RP rocket motor. The design study was constrained by assuming the generator must function within the performance and structural limits of an existing magnet and by assuming realistic limits on (1) the axial electric field, (2) the Hall parameter, and (3) current density, and (4) heat flux (given the criteria of heat sink operation). The major results of the work are summarized as follows:

- A Faraday type of generator with rectangular cross section is designed to operate with a combustor pressure of 300 psi. Based on a magnetic field strength of 1.5 Tesla, the electrical power output from this generator is estimated to be 54.2 KW with potassium seed (weight fraction 3.74%) and 92 KW with cesium seed (weight fraction 9.66%). The former corresponds to a enthalpy extraction ratio of 2.36% while that for the latter is 4.16%.
- A conceptual design of the Faraday MHD channel is proposed, based on a maximum operating time of 10 to 15 seconds. This concept utilizes a phenolic back wall for inserting the electrodes and inter-electrode insulators. Copper electrode and aluminum oxide insulator are suggested for this channel.
- A testing configuration for the sub-scale rocket based MHD system is proposed.

An estimate of performance of an ideal rocket based MHD accelerator is performed. With a current density constraint of 5 Amps/cm^2 and a conductivity of 30 Siemens/m, the push power density can be 250, 431, and 750 MW/m^3 when the induced voltage uB have values of 5, 10, and 15 KV/m, respectively.

1. INTRODUCTION

The concept of coupling a rocket motor with magnetohydrodynamic (MHD) devices was proposed several decades ago.[1,2,3,4] The is due to not only that rocket motors are an appropriate plasma source (after seeding) for MHD applications but also a simple structured, light weight MHD device is feasible. Recently, there has been a resurgent interest in MHD aerospace applications, in which system weight is always a major concern. Rocket based MHD system is considered a good candidate to fit in these aerospace applications. A couple of rocket based MHD systems have been proposed. Among them, some were for electric power generation,[5,6,7] others for flow acceleration,[8,9] or even a combination of both.[10]

The present rocket based MHD generator design study is deemed as the first phase of a research project for developing such a system. Next phase will be fabrication and laboratory test for the rocket MHD system design concluded in the present study. Sub-scale rocket motors with 300 or 1000 psi combustion pressure of NASA Marshall Space Flight Center (MSFC) and a magnet system used in early MHD generator studies at Energy Conversion Facility (ECF) of The University of Tennessee Space Institute (UTSI)[11] are proposed to be used in the next phase laboratory set up. Due to certain practical limitations associated with these rocket motors and the magnet system, the rocket based MHD generator designed herein might not show great performance. The major goals of the entire research project are to demonstrate power production from the designed generator, to set up a data base for verification of analytical modeling work, and to accumulate experience in designing and operating an MHD generator of this kind. Once these goals are reached, large scale rocket based MHD generators can be later designed to provide great performance with confidence.

This report overviews work performed on the rocket based MHD generator design study contract awarded to ERC. Inc. from NASA Marshall Space Flight Center. Possibilities to examine rocket based MHD accelerator are resumed through the entire research project.

2. LOx/RP ROCKET MOTOR THERMO/PLASMADYNAMIC CHARACTERIZATION

The MHD generator envisioned in this study is based on sub-scale LOx/RP rocket motors available at the Marshall Space Flight Center. With the same nozzle geometry, these rocket motors can be divided into two categories according to combustion pressures, e.g. 300 and 1000 psia. Mass flow rates, thrust, exit temperature, and pressure of these two kinds of rocket motors burning with 50/50 of LOx/RP were calculated using NASA thermo-chemical equilibrium code (SP-273)[12] and listed in Table 1 along with important geometrical factors. The thrust thus obtained assumed ideal expansion to vacuum. Sketch of the 500 pound thrust liquid fuel rocket motor is shown in Figure 1.

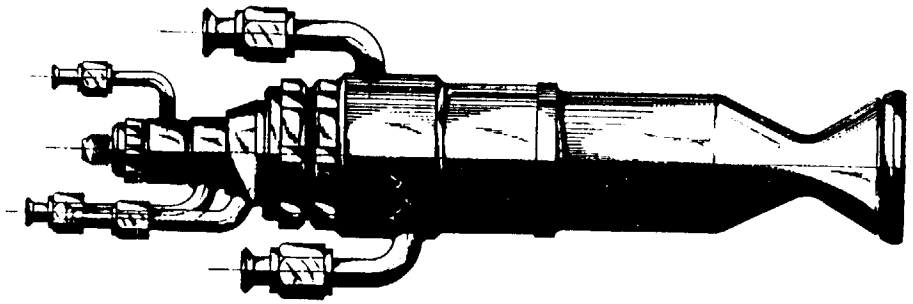

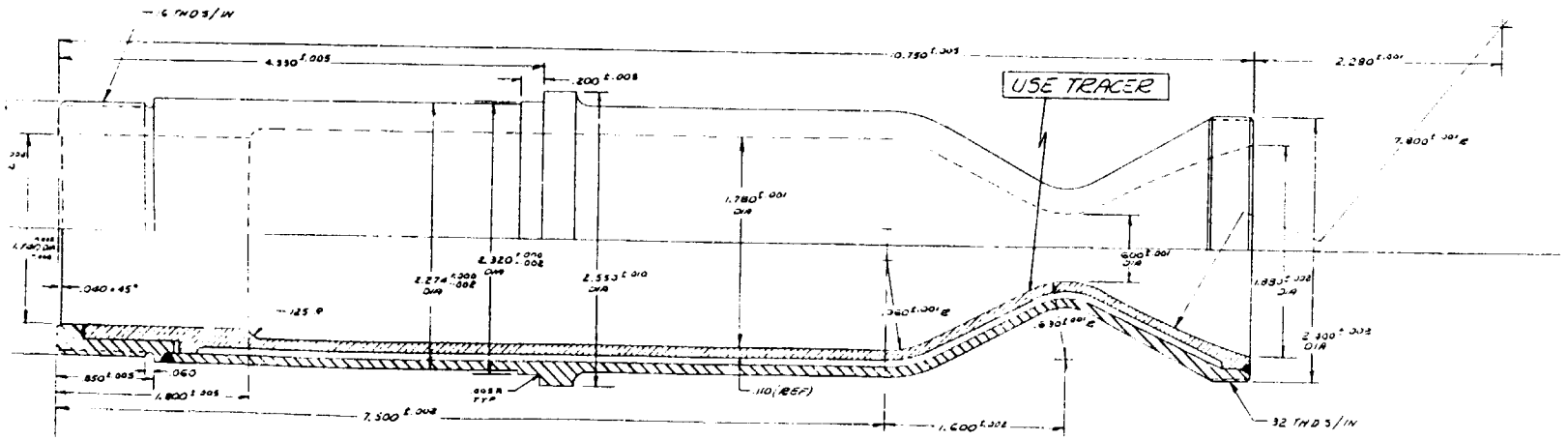

Figure 1 Sub-Scale Rocket Motor of MSFC (SNTL - D - 500 - 1000, Liquid Fuel)

Stagnation Pressure (psi)	300	1000
Stagnation Temperature (K)	3473	3634
Throat Diameter (in)	0.6	0.6
Nozzle Exit Diameter (in)	1.88	1.88
Exit Temperature(K)	2160	2126
Exit Pressure (atm)	0.295	0.953
Exit Mach No.	3.09	3.14
Throat Sonic speed (m/s)	1170.	1191
Mass Flow Rate(kg/s)	0.211	0.695
Thrust (lb_f)	150	500

Table 1. Geometry and Theoretical Performance of MSFC's Sub-scale Rocket Motors

The primary objective of the present design study is to reach a conceptual design of a rocket based MHD system which produces maximum power output based on MSFC's sub-scale rocket motors and ECF magnet system. Treating the MHD generator as additional payload to the rocket system, a compact MHD device is preferred. To minimize the weight of an MHD channel, the power density, defined as the electrical power output per unit of internal volume, of the generator has to be maximized.

It is widely known that power density of an MHD generator is proportional to the product of the plasma conductivity with the squares of the plasma velocity and imposed magnetic field strength. That is

$$Power\ Density \sim \sigma u^2 B^2 \tag{1}$$

where σ is the electrical conductivity of plasma, u is the velocity, and B is the magnetic field strength. To maximize MHD performance, the highest power density possible needs to be maintained in the channel of an MHD generator.

2.1 Seeding

From the temperature range shown in Table 1, a LOx/RP rocket motor requires seeding its combustion gas with an easily ionized alkali salt to provide high conductivity plasma. Applications of cesium hydroxide (CsOH) or potassium hydroxide (KOH) as the seeding component is examined in this design study. Figure 2 presents calculated plasma conductivities at the combustor conditions for various weight percentages of potassium and cesium. As indicated in the figure, peak value of conductivity exists in each curve. For example, the conductivity maximizes at 5.2% and 16.5% for potassium and cesium respectively at combustor pressure of 300 psi. Cesium seeding provides higher plasma conductivity than potassium by virtue of its lower ionization potential.

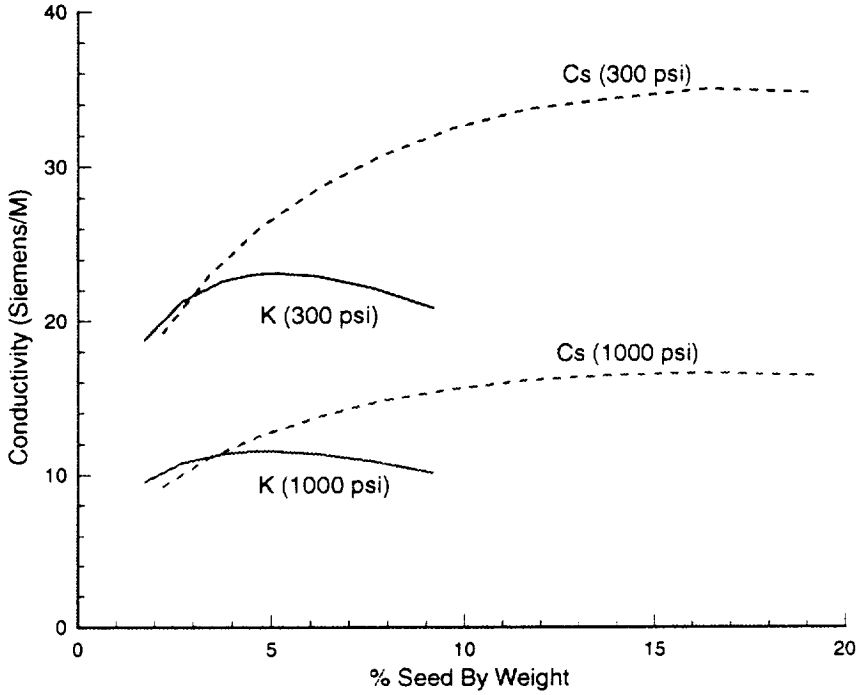

Figure 2 Plasma Conductivity Variation with Seeding Percentage of Potassium and Cesium at Various Combustion Conditions of LOx/RP Rocket Motors.

On the other hand, cesium is extremely toxic and causes concerns of environmental pollution when exhausted by a rocket. Also cesium is considerably more expensive than potassium. Therefore, potassium is selected as the primary seeding component herein. Cases using cesium as seed would also be considered in this investigation as a maximum effort to achieve a high power density by maximizing the plasma conductivity when only limited magnetic field strength is available.

2.2 Generator Entry Point Selection

It is convenient to further subdivide the expression (1) of power density into the terms B^2 and the product $\frac{\sigma u^2}{4}$ where the latter is termed as the power density parameter. The power density parameter is a plasma characteristic. From its definition, the plasma conductivity is an exponentially increasing function with temperature while plasma velocity is approximately a decreasing square root function with temperature in a nozzle flow.

The potential to produce electrical power in the expanded plasma states is of primary importance for a rocket based MHD power system. During the expansion, the plasma temperature and pressure drop while its velocity increases. While the plasma conductivity increases with decreasing pressure at constant temperature, the temperature dependence is strong and dominant so that the conductivity in general decreases as the plasma expands to higher speed. That is, the power density parameter is closely related with plasma temperature and exhibits an optimal value when plasma flowing through a rocket nozzle. Along the expansion section of nozzle, the point where the optimal power density exists is a good choice as the entry of MHD channel to ensure maximum MHD performance.

Figures 3 and 4 are the power density parameter mappings for potassium and cesium respectively produced by varying both the seeding percentage and the expansion ratio when the combustion pressure is 300 psi.. For potassium, the peak value of power density parameter is found at 3.74% seed and expansion ratio of 8.0 while, for cesium, it is located at 9.66% seed and expansion ratio of 14.1. The former expansion ratio (for potassium) is less than that of MSFC's rocket but the latter (for cesium) is greater, according to the geometry listed in Table 1. In practice, a relatively wide range of expansion ratio can be selected without too much reduction. For example, along the curve of 3.74% potassium seeding in Figure 3, the expansion ratio can be chosen anywhere between 6 to 10 with less than 1.2% decrease in power density parameter from its peak value. From the 9.66% cesium seeding line in Figure 4, any expansion ratio between 9.5 to 20 can be used if 1.2% reduction in power density parameter relative to its optimal value is allowable.

For 1000 psi combustor pressure, the peak power density parameter occurs at about the same seed percentage and expansion ratio as that for 300 psi case for both potassium and cesium. Keeping the same seeding percentage, variations in the expansion ratio between 6 to 10 for potassium and between 9.5 to 20 for cesium result in less than 1.5% drop in power density parameter with respect to its peak value.

3. DESIGN ANALYSIS

Two major types of MHD generator in terms of loading configurations are Faraday and Hall types, as shown in Figure 5. Electrode pair of a Hall generator is in the flow direction (i.e., x-direction) while that of a Faraday generator is perpendicular to the flow train (i.e., y-direction). With segmented electrodes, axial electrical currents (also named as Hall currents) inside a Faraday generator can ideally be neutralized and only Faraday currents flow through the electrodes. With an externally applied magnetic field in the z-direction, the induced Lorentz force from MHD interaction will lie in direction against flow train in a Faraday type of generator to decelerate the flow and convert the flow kinetic energy into the electrical energy.

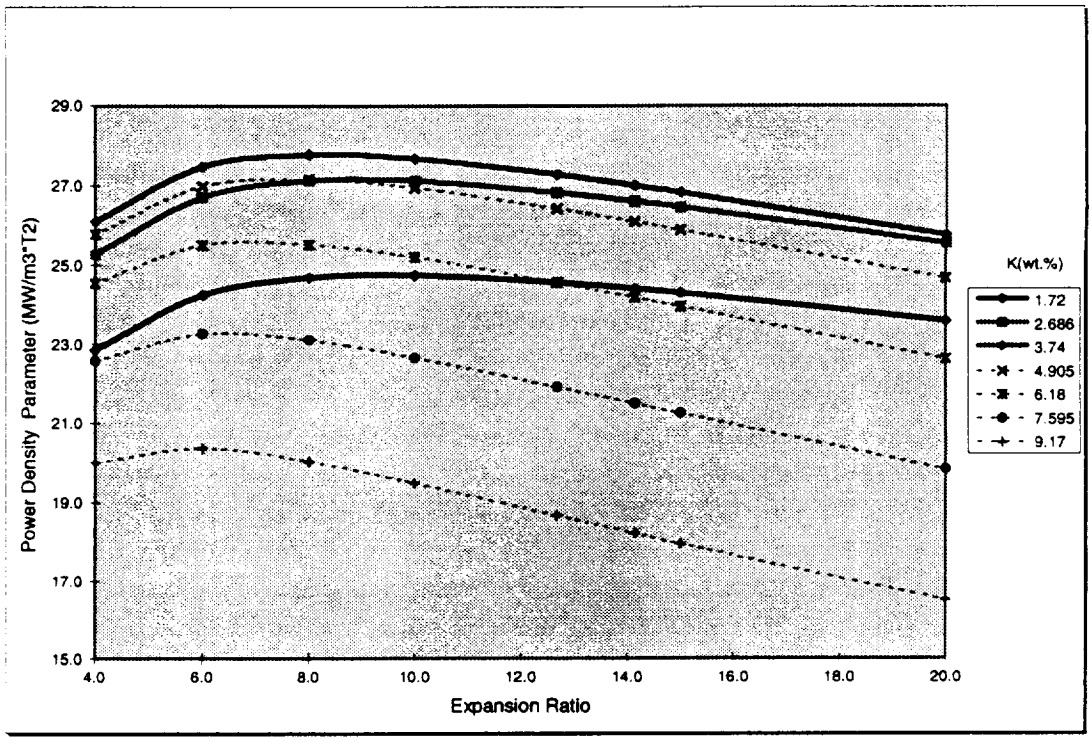

Figure 3 Power Density Parameter Distribution along 300 psi LOx/RP Rocket Nozzle with Different Potassium Seeding Percentages.

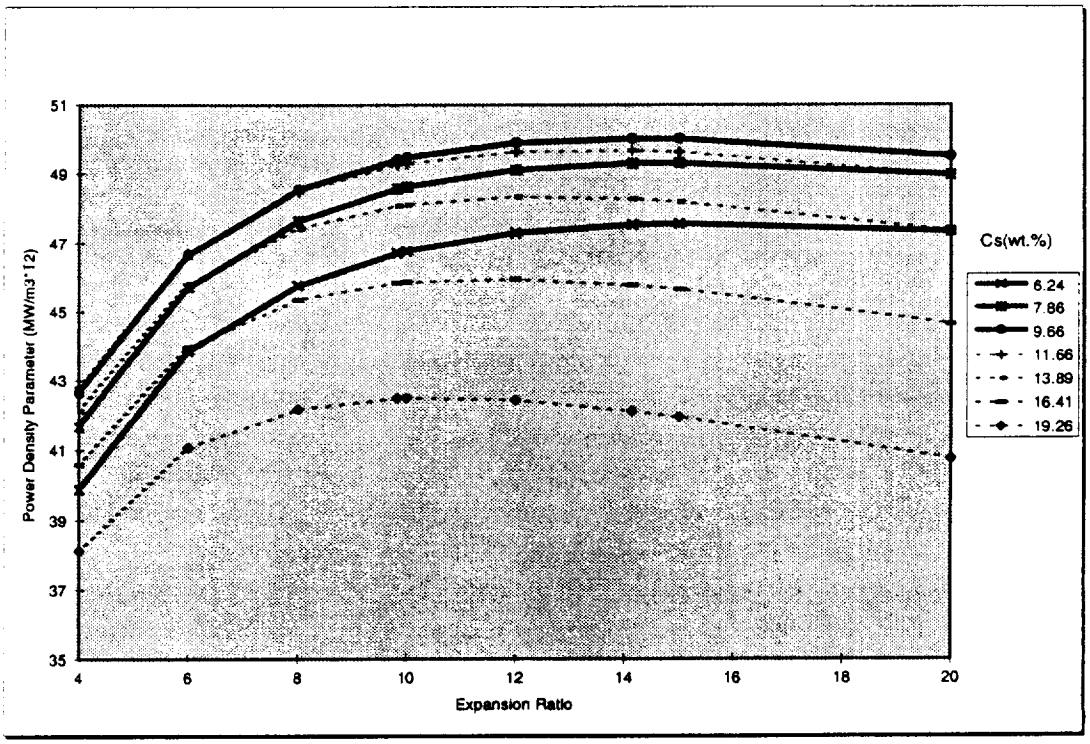

Figure 4 Power Density Parameter Distribution along 300 psi LOx/RP Rocket Nozzle with Different Cesium Seeding Percentages.

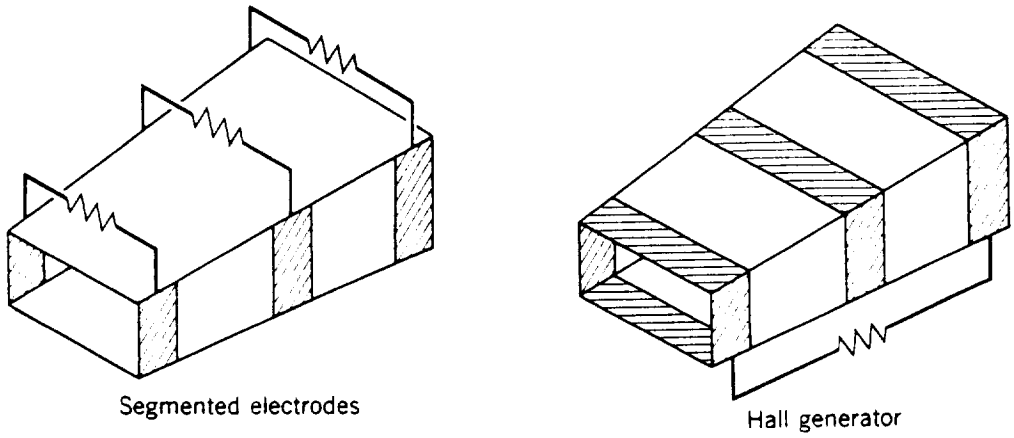

Figure 5 Loading Configuration of a Faraday Generator with Segmented Electrodes and a Hall Generator

On the other hand, the wall of a Hall generator is shorted, currents in the axial direction are that flow through the electrodes. With a magnetic field in the z-direction, the Lorentz force in a Hall generator has a component perpendicular to the flow train and creates a side force against the channel wall. This side force, if significant in magnitude, might perturb the flow train, cause boundary layer separation, and make a rocket to turn, when a rocket based MHD generator employs a Hall configuration. Based on the operating conditions of MSFC's sub-scale rocket motor, an order of magnitude estimate of Lorentz force in a Hall generator is carried out below.

Axial current density, j_x , in a Hall generator is calculated as

$$j_x = \frac{\omega\tau}{1+\omega\tau^2}(1-K_H)\,\sigma\,u\,B \tag{2}$$

where $\omega\tau$ is Hall parameter defined as the ratio between electron cyclotron frequency and electron collisional frequency with atoms, molecules, and ions. K_H is the loading factor of a Hall generator.

To balance the Lorentz force, a pressure force, Δp_y, in the y-direction will form as

$$\frac{\Delta p_y}{\Delta y} \approx j_x\,B \tag{3}$$

Combining expressions (2) and (3), the order of Δp_y can be estimated by

$$\Delta p_y \approx \frac{\omega\tau}{1+\omega\tau^2}(1-K_H)\,\sigma\,u\,B^2\,\Delta y \tag{4}$$

In a sub-scale rocket based MHD generator, typical values for variables in the right hand side of expression (4) are $\omega\tau \approx 5$, $K_H \approx 0.5$, $\sigma \approx 20$ Siemens/m, $u \approx 2500$ m/s, B 2 T, and $\Delta y \approx 0.1$ m. From these, we can get $\Delta p_y \approx 2000$ pa. With a density $\rho \approx 0.03$ kg/m^3, ratio between this Lorentz induced pressure force and dynamic pressure in the flow train is about $1x10^{-2}$. Therefore, we can conclude that the side force induced by MHD interaction in a sub-scale rocket based Hall generator does not perturb the flow train significantly.

An MHD generator of Hall configuration has simpler structure compared to one of the Faraday type since only one single electrode pair and single load is needed in a Hall generator. This simplicity makes Hall configuration more attractive in applications where system weight is of primary importance, even though a linear Hall generator is usually less efficient than one of Faraday type. On the other hand, it is noticed that the side force induced by Hall current is negligible only for small scale MHD generators. For a full scale MHD scale, Δy can be one order of magnitude larger and, under such circumstances, the Lorentz induced side force is no longer negligible. Therefore, a Faraday type of generator is suggested in the present study.

3.1 Magnet Constraints

For cost savings, an existing magnet will be used in the experimental hardware set up following this design study. Therefore, it is necessary to size the experiment before detailed calculations for the MHD generator channel can be performed. This is contrast to conventional MHD design practice. In a conventional design process, the guiding criteria for the generator channel are couched in terms of plasma mass flow and electrical conductivity available as well as power output sought. Subsequent for the final channel configuration, the magnet is constructed to match the required field strength and interaction length. In the present study, the procedure is to accommodate an MHD channel within an existing magnetic field envelop.

The magnet proposed to be used in the follow up experiment is the existing ECF's magnet at UTSI. This magnet is a conventional water-cooled electromagnet with a C-frame core. The pole gap is 10 cm and the pole faces were originally rectangular shape (91.44 cm x 15.2 cm) and later on modified to a trapezoidal shape. This magnet was originally powered by DC welders and provided a maximum field strength of 2.2 Tesla.

Figure 6 shows the normalized magnetic induction along the magnet axis. The magnetic field distribution is relatively flat nearby its peak for a distance approximately 20 to 24 inches. In order to maximize power density, which is proportional to the square of the field strength, it is desirable to have a uniform high strength field. The generator must be able to fit within the volume with uniform field. In the present design, the constant field strength is selected to be 1.5 Tesla and the effective length of the MHD channel is 20 inches, evenly divided into 20 electrode pitches. This level of magnetic field strength is believed to be achievable after rebuilding the magnet system, even though it has been out of service since early 80's.

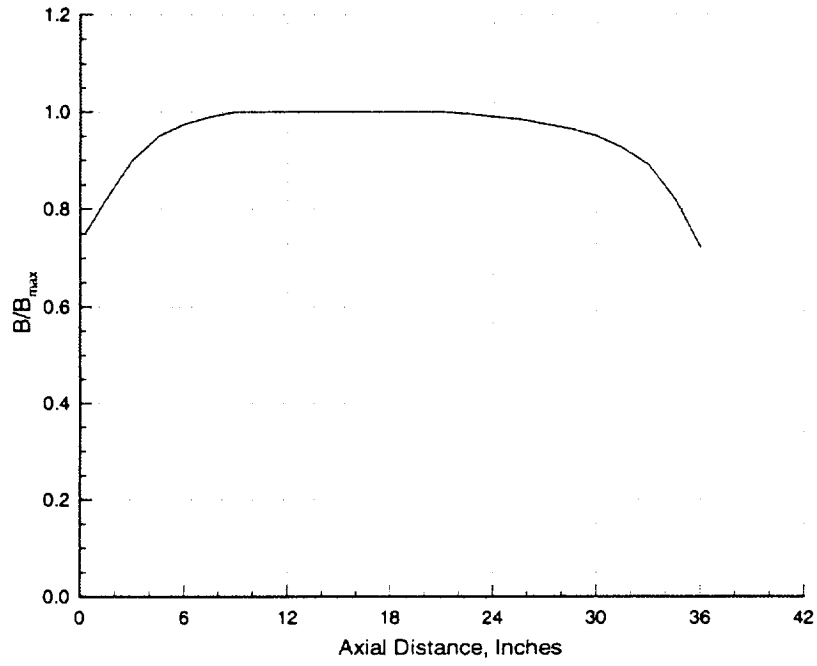

Figure 6 Normalized Magnetic Flux Density Distribution of ECF Magnet

For sake of machining simplicity and cost saving, an MHD channel with circular cross section was thought to be a possible candidate for designing a rocket based MHD generator where rocket combustor and nozzle are of circular shape. Reference ? is an example for applying such a circular cross section channel. In the present design, due to the narrowness of the magnet pole gap (~ 4 inches), circular cross section is impossible to feed the necessary mass flow rate, taking into considerations of the thickness of channel walls. The generator designed can only have a rectangular channel with a constant width but diverging in its height. Matching a cylindrical rocket to a rectangular channel requires a transition nozzle which accomplishes the cross-sectional shape transition. This transition nozzle has to be carefully designed and fabricated to avoid corner interference and subsequently flow non-uniformity.

3.2 Other Constraints

For a Faraday generator with segmented electrodes, the electrical field in the axial direction has to be limited to avoid happening of electrode arcing phenomena. Once arcing occurs, the adjacent electrodes can be shorted to degrade the generator performance. The locally high dissipation from highly concentrated arcing discharges might result in erosion of the electrode surface and shorten the channel operating life. In the design, the axial electrical field is limited to below 40 volts/cm by adjusting the generator loading.

The plasma in the MHD channel is better to operate under a critical Hall parameter. If Hall parameter exceeds to its critical value, eddy currents appear in plasma and large scale plasma non-uniformities form in the channel. These non-uniformities increase the plasma internal impedance and subsequently lower the generator performance. The critical Hall parameter is selected to be 4.

Faraday currents generated in the generator flow to the external loads through electrodes. The Faraday current density has to be constrained below a certain value, depending on electrode material and geometry, to avoid excessive heat generated on electrode surface and subsequently cause damage to the electrodes. An upper limit of 5 A/cm^2 in current density is adopted in this design study.

Since no water-cooled mechanism is planned in the designed MHD generator, the channel wall has to serve as heat sink. To prevent burning down of the channel, heat flux through the channel has to be limited. For an operation time of 10 to 20 seconds using aluminum oxide as the insulator in the MHD channel, heat flux is restricted to below 300 watts/cm^2.

3.3 Generator Performance

The design calculations are performed by using an ERC's in-house MHD generator computer code, GEN-1D. This computer code is based on a one dimensional generator flow model which approximates the influence of the boundary layer in the plasmadynamic calculation. However, this computer model does include a direct accounting for the boundary layer in its modeling of the generator electrical performance. The local voltage drop across the boundary layer is determined by assigning the normalized voltage drop factor, Δ, defined as $V_d / (u\ B\ h)$, where V_d is the effective voltage drop and h is the channel height. For small generator, Δ is typically 0.3,[14] this will reduce the generator efficiency by 30% and power density by a factor of 2.

In GEN-1D, the real gas equation of state is provided by a prior combustion calculations utilizing the NASA SP-273 thermo-equilibrium computer program.[12] This program computes the thermo-equilibrium process to provide a real gas Mollier chart which is utilized in GEN-1D to determine state points through either user defined curve fits or chart interpolation. All the thermodynamic variables are fit as functions of pressure and temperature. The combustion calculations include solution for the plasma electrical transport properties.[13] Both electrical conductivity and mobility are also represented as functions of the local thermodynamic states (pressure and temperature). Using GEN-1D, the flow can also be assumed to act like a chemically and vibrationally frozen flow.

Using GEN-1D, parametric studies of generator performance are performed as a significant part of generator design. These studies considered parametric variations of inlet Mach number and channel geometry while other parameters treated as fixed value variables are listed in Table 2.

Mass Flow Rate (kg/s):	
Combustor Pressure 300 psi	0.228 (potassium)
	0.235 (cesium)
Combustor Pressure 1000 psi	0.75 (potassium)
	0.77 (cesium)
Seeding Percentage (wt.%)	3.74 (potassium)
	9.66 (cesium)
Magnetic Field Strength (Tesla)	1.5
Effective MHD Channel Length (inch)	20
Electrode Pitch (inch)	1
Diffuser Exit Pressure (atm)	1
Channel Wall Temperature (K)	600
Wall Roughness (mm)	0.03
Prandtl Number	0.7

Table 2. Fixed Value Parameters Applied in Faraday Generator Design

For each electrode pair, loading factor K, defined as the ratio of external load resistance to the sum of external and plasma resistance, is initially set to its optimum value for producing maximum electrical power, i.e. 0.5. If the constraint of axial electrical field or that of Faraday current density is violated, loading factor will be increased to satisfy the constrain.

Chemical non-equilibrium effects become significant in high speed nozzle flows. GEN-1D does not have the capability of treating these non-equilibrium effects. Instead, for each design case, calculations are performed with both chemically equilibrium and frozen flow assumptions and their results are compared. Frozen flow calculations are activated downstream to the point where local Mach number reaches 2.4 in the nozzle.

A summary of the findings obtained from the parametric studies are:

1. An MHD generator with constant velocity was thought to be a good configuration to resume the rocket thrust, it turns out to be too much expansion in the MHD channel (expansion ratio ≥ 10) after certain trials. Constant Mach number channel is a better starting point.
2. The MHD interaction is a strong function of combustor pressure due to plasma conductivity level. Cases with combustor pressure of 1000 psi are unable to satisfy both constraints of magnet size and heat flux simultaneously.
3. The generator inlet Mach number has to be high enough to reduce the flow temperature to limit heat loss rate.

Starting from a constant Mach number channel design, Figure 7 shows the distributions of important flow and electrical properties, as well as heat transfer rate in such an MHD channel with potassium seed. The channel inlet has a area expansion ratio of 8 with respect to the nozzle throat and the combustor pressure is 300 psi. The results show that too much expansion in the MHD channel (expansion ratio = 6.5), the pressure drops very fast, as a result, the Hall parameter exceeds the design criteria in the downstream portion of channel. This large Hall parameter causes strong axial electric field and the loading parameter is adjusted from its optimum value to limit the local electric field, which reflects in the plateau in the Hall E-field distribution. Also, relative high plasma temperature at the inlet induces a locally high heat flux, breaks the design constraint too. Even though these conclusions are obtained under the assumption of thermo-chemical equilibrium, the results found by using a frozen flow assumption also show the same trend and are thus omitted from listing herein.

Next, efforts focus on removing those violations in design constrains. In practice, the channel contour is linear for simplicity of fabrication and side walls should be designed with a constant slope (i.e., constant wall angle). Smaller wall angles are chosen to limit flow expansion within the MHD channel. A higher inlet Mach number is selected to locally decrease the flow temperature and the associated heat flux value. After all the designing constraints are followed, adjustments in the aspect ratio of channel cross section are carried out to provide more allowance in the magnet pole gap for the channel wall thickness. Thicker walls provide better heat sink effects. During the parametric study, the generator performance and the resultant thrust of the rocket based MHD system are of primary concerns. That is to say, the goal of the parametric study is to search for an optimum group of design parameters for an MHD generator based on an existing rocket motor and magnet. This optimum design parameter combination satisfies all the design constraints and, at the same time, produces electric power as much as possible and minimizes the influences on the thrust of the rocket system.

After several adjustments, the designed channel geometry is obtained and included in Figure 8. The constant width MHD channel has a square cross section at inlet (1.67 x 1.67 inches) and an expansion half angle of 4 degree. At inlet, the area expansion ratio is 9.82 with respect to the nozzle throat.

Figures 9-12 and Table 3 summarize the predicted generator design performance for a potassium seeded MHD generator with a 300 psi combustion pressure. Following an expansion flow, temperature drops and charged particles (ions and electrons) of a plasma recombine. For an expanding plasma, frozen effects prevent recombination and the associated energy release. As a result, a frozen plasma flow under expansion reserve higher conductivity but lower plasma temperature than an equilibrium expansion flow. This frozen effect can easily be observed when comparing data shown in Figure 9 to that given in Figure 10. Stronger MHD interaction, higher electrical power, and lower heat loss are induced by frozen effects.

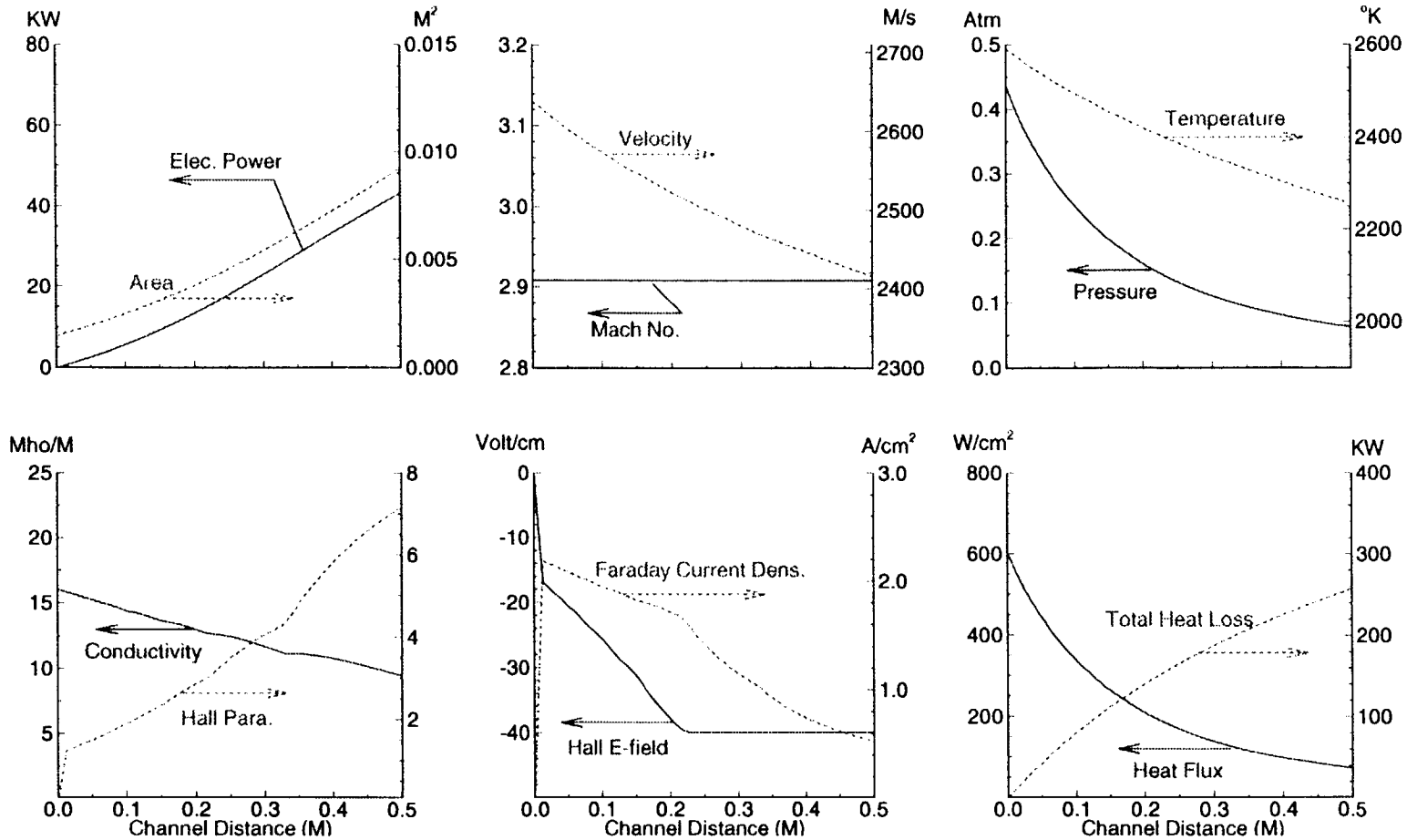

Figure 7 Calculated Flow and Electrical Parameter Distributions for the Constant Mach Number Faraday Generator. RP1 + O2 + KOH, K(wt.%) = 3.74, $P_{comb.}$ = 300 psi, B = 1.5 T, Mass Flow = 0.228 Kg/s, $A_{MHD,inlet}/A_{throat}$ = 8., Channel Length = 20 inches. (Equilibrium Flow Assumption)

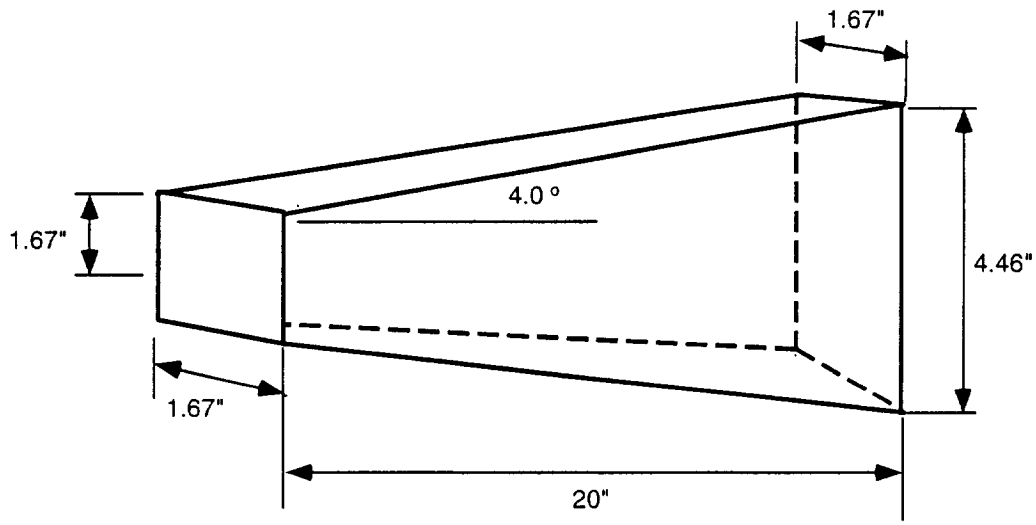

Figure 8 Geometry of the Designed MHD Channel

In real life design, it is reasonable to assume that the predicted MHD performance of a designed generator falls between the gap calculated separately by equilibrium and frozen assumptions. Average values of results obtained from these two extremes, equilibrium and frozen, are deemed as acceptable design values for the generator geometry proposed in the present design study. Use of these average values is supported by comparisons of different MHD parameters given in Figures 11 and 12, that is, the gap between two extremes of each parameter listed is not wide.

Therefore, the predicted power output for the proposed MHD generator is 54.2 KW, with potassium seed and 300 psi combustor pressure. The power extraction corresponds to an enthalpy extraction ratio of 2.36%. The thrust for this rocket based MHD system is estimated to be 90 lb_f, assuming ideal expansion to atmosphere after the generator exit.

Once cesium hydroxide is used as seed component in the proposed rocket based MHD system, the theoretically predicted performance are summarized and included in Table 4 and Figures 13-16. Comparison between the results given in Figure 14 to that in Figure 13, relative to the equilibrium calculations, stronger MHD interaction of the frozen flow assumption only available in the upstream portion of the MHD channel. Too fast flow velocity drop in the upstream portion results in relatively lower MHD interaction in he downstream part and the total enthalpy extraction ratio of frozen flow assumption is lower than that for equilibrium flow assumption.

Obviously, due to higher conductivity of cesium plasma, the MHD interaction in the channel becomes stronger and the generator performance improves, relative to that obtained with potassium seed. The estimated power produced by the same rocket based MHD system using cesium is 92 KW, equivalent to an enthalpy extraction ratio of 4.16%, and the thrust becomes 72.6 lb_f when expands to atmosphere isentropically.

	Equilibrium	Frozen
Total Mass Flow Rate	0.228	0.228 kg/s
Thermal Input	2.24	2.35 MW
Entrance Total Pressure	21.2	19.8 atm
Exit Total Pressure	6.69	4.61 atm
Entrance Total Temperature	3713	3623 K
Exit Total Temperature	3419	3290 K
Generator Length	20	20 inches
Generator Mean Flow Area	0.00333	0.00333 m^2
Generator Volume	0.0017	0.0017 m^3
Internal Surface Area	0.123	0.123 m^2
Average Heat Flux	-154	-148 W/cm^2
Mean Static Temperature	2448	2370 K
Mean Velocity	2639	2571 m/s
Mean Mach Number	3.02	2.92
Mean Conductivity	13.8	21.4 Mho/m
Mean Hall Parameter	2.62	2.74
MHD Power	43.7	64.7 W
Specific Power Output	0.192	0.283 MW/kg
Interaction Parameter (Ip)*	0.723	1.06
Power Density	25.8	38.2 MW/m^3
Enthalpy Extraction	1.95	2.76 %
Generator Efficiency	19.9	27.5 %
Electrical Efficiency	36.5	36.4 %
Open Circuit E-field	2.77	2.70 kV/m
Short Circuit Current	20.5	31.0 A
Internal Impedance	68.5	44.2 Ohms
Joule Heat Dissipation	42.0	62.2KW
MHD Push Power	-120	-178 KW

* MHD Interaction Parameter Based Upon Pressure, $I_p = \int_0^t \frac{\bar{J} \times \bar{B}}{p} dx$.

Table 3. Predicted MHD Generator Performance (Potassium Seed, $P_{comb.}$ = 300 psi)

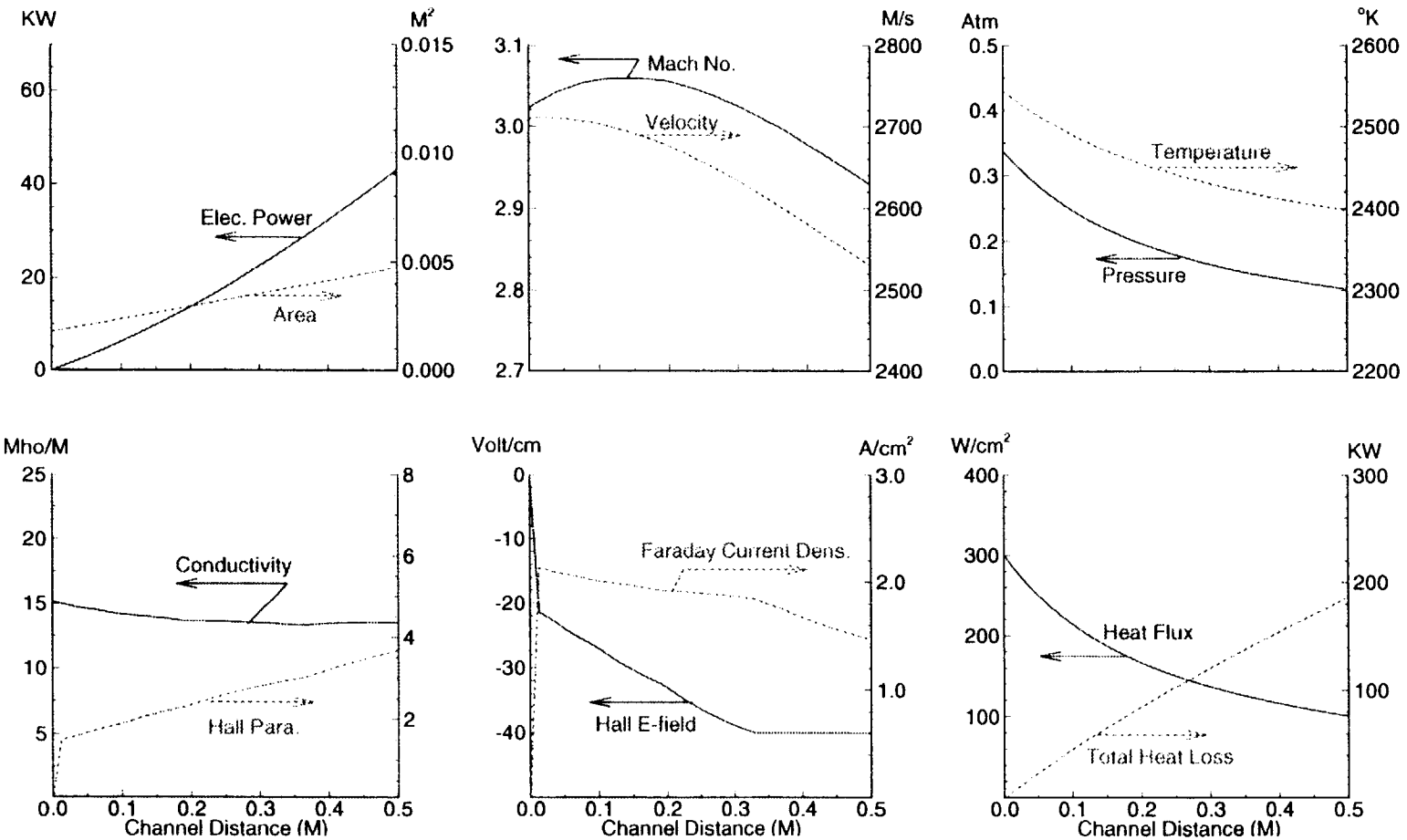

Figure 9 Calculated Flow and Electrical Parameter Distributions for the Designed 4° Half Wall Angle Faraday Generator. RP1 + O2 + KOH, K(wt.%) = 3.74, $P_{comb.}$ = 300 psi, B = 1.5 T, Mass Flow = 0.228 Kg/s, $A_{MHD,inlet}/A_{throat}$ = 9.82, Channel Length = 20 inches. (Equilibrium Flow Assumption)

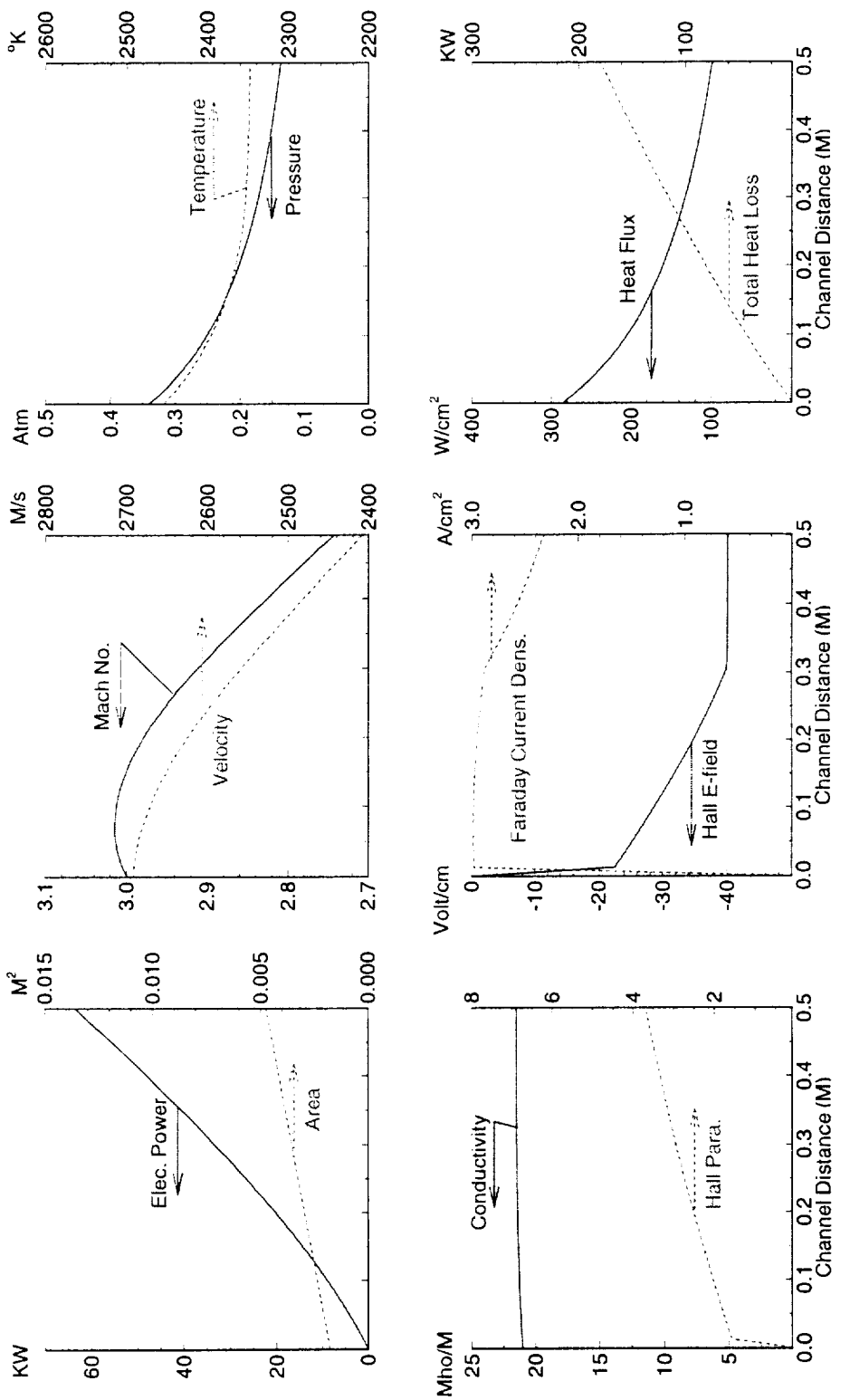

Figure 10 Calculated Flow and Electrical Parameter Distributions for the Designed 4° Half Wall Angle Faraday Generator. RP1 + O2 + KOH, K(wt.%) = 3.74, $P_{comb.}$ = 300 psi, B = 1.5 T, Mass Flow = 0.228 Kg/s, $A_{MHD.inlet}/A_{throat}$ = 9.82, Channel Length = 20 inches. (Frozen Flow Assumption)

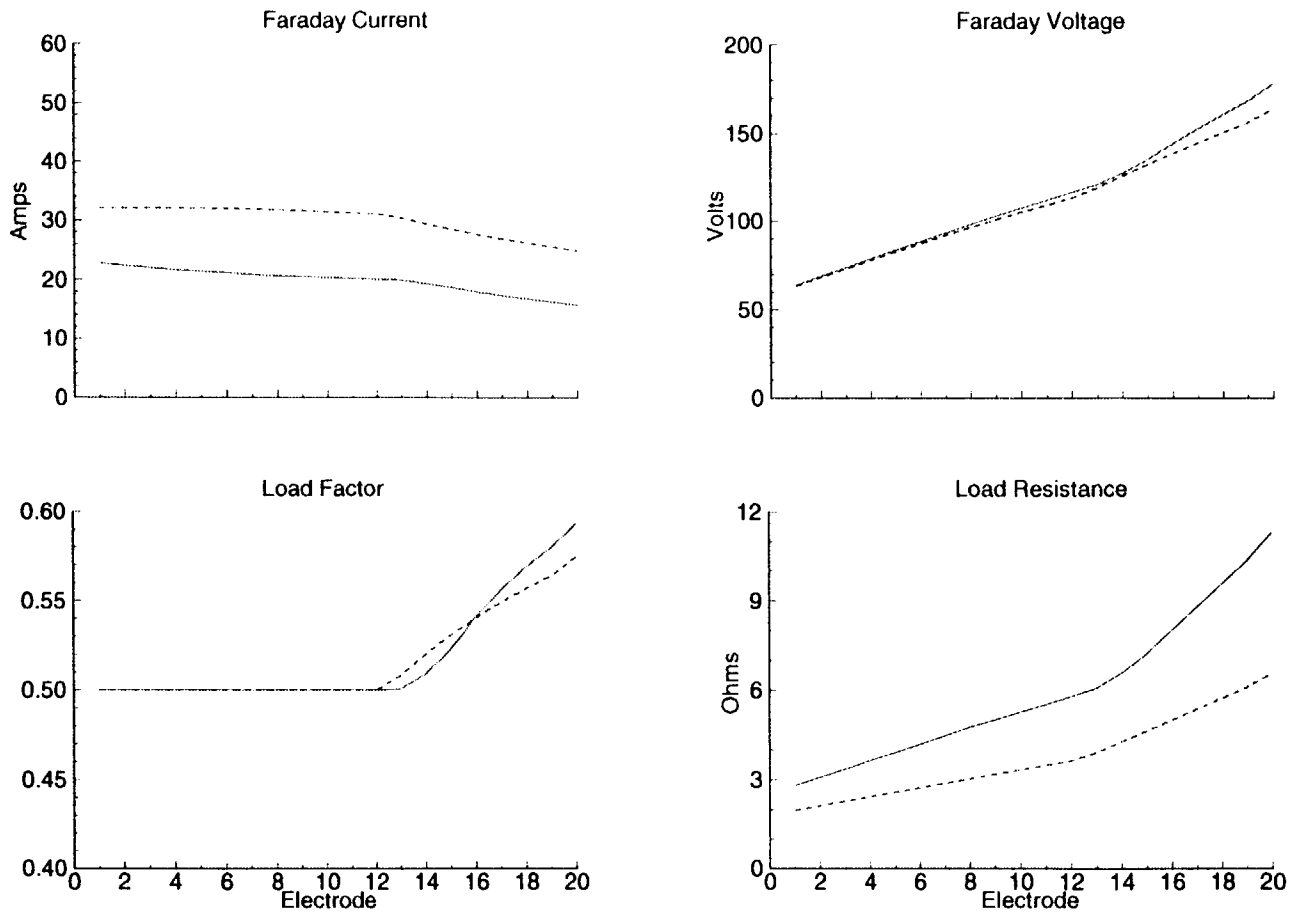

Figure 11 Loading Conditions for the Designed 4° Half Wall Angle Faraday Generator Using Potassium Seed. (Solid Lines: Equilibrium Flow, Dashed Lines: Frozen Flow)

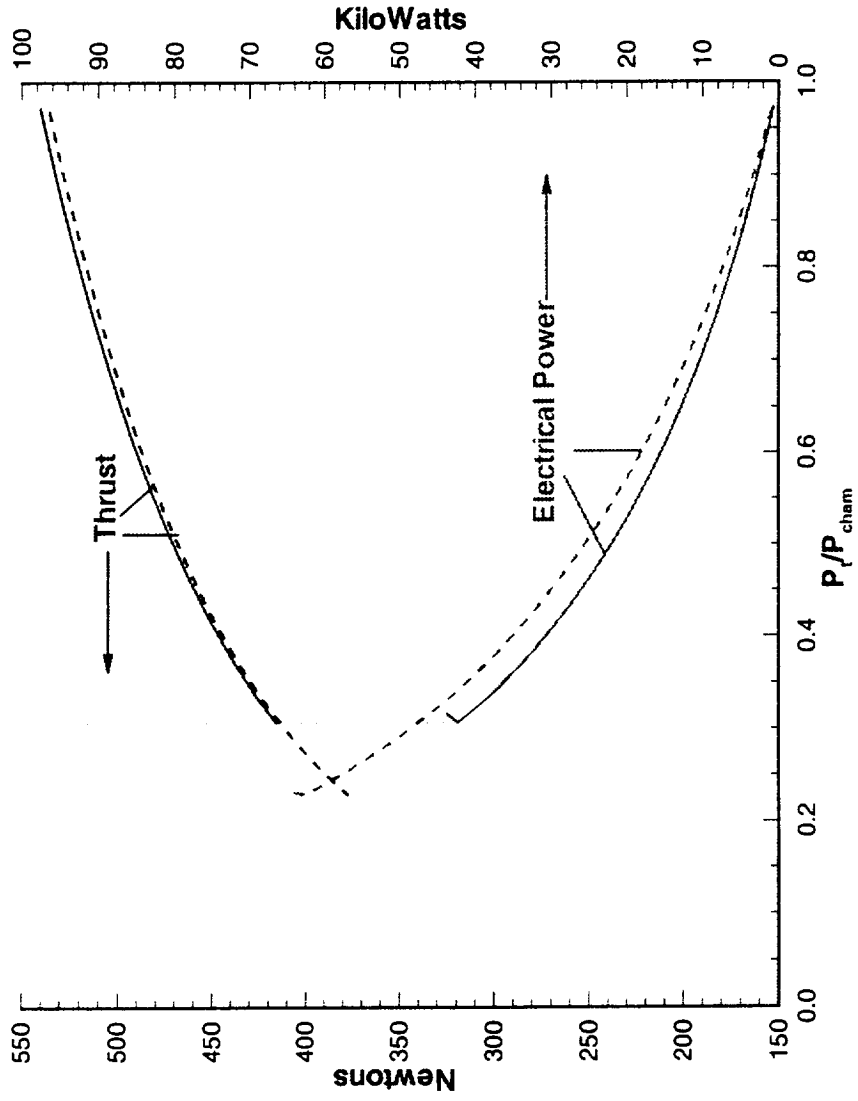

Figure 12 Relation between Thrust, Electrical Power, and Total Pressure Loss in the Channel of the Designed Rocket Driven MHD Generator Using Potassium Seed. (Solid Lines: Equilibrium Flow, Dashed Lines: Frozen Flow)

	Equilibrium	Frozen
Total Mass Flow Rate	0.235	0.235 kg/s
Thermal Input	2.14	2.28 MW
Entrance Total Pressure	21.2	19.8 atm
Exit Total Pressure	3.23	2.83 atm
Entrance Total Temperature	3731	3641 K
Exit Total Temperature	3285	3252 K
Generator Length	20	20 inches
Generator Mean Flow Area	0.00333	0.00333 m^2
Generator Volume	0.0017	0.0017 m^3
Internal Surface Area	0.123	0.123 m^2
Average Heat Flux	-128	-147 W/cm^2
Mean Static Temperature	2506	2432 K
Mean Velocity	2447	2402 m/s
Mean Mach Number	2.85	2.78
Mean Conductivity	32.5	35.9 Mho/m
Mean Hall Parameter	2.39	2.58
MHD Power	89.7	94.0 W
Specific Power Output	0.382	0.400 MW/kg
Interaction Parameter (Ip)*	1.53	1.64
Power Density	53.0	55.5 MW/m^3
Enthalpy Extraction	4.19	4.13 %
Generator Efficiency	37.5	35.5 %
Electrical Efficiency	35.0	35.0 %
Open Circuit E-field	2.57	2.52 kV/m
Short Circuit Current	44.7	48.7 A
Internal Impedance	29.2	26.3 Ohms
Joule Heat Dissipation	90.2	97.1KW
MHD Push Power	-0.256	-269KW

* MHD Interaction Parameter Based Upon Pressure, $I_p = \int_0^l \frac{\bar{J} \times \bar{B}}{p} dx$.

Table 4. Predicted MHD Generator Performance (Cesium Seed, $P_{comb.}$ = 300 psi)

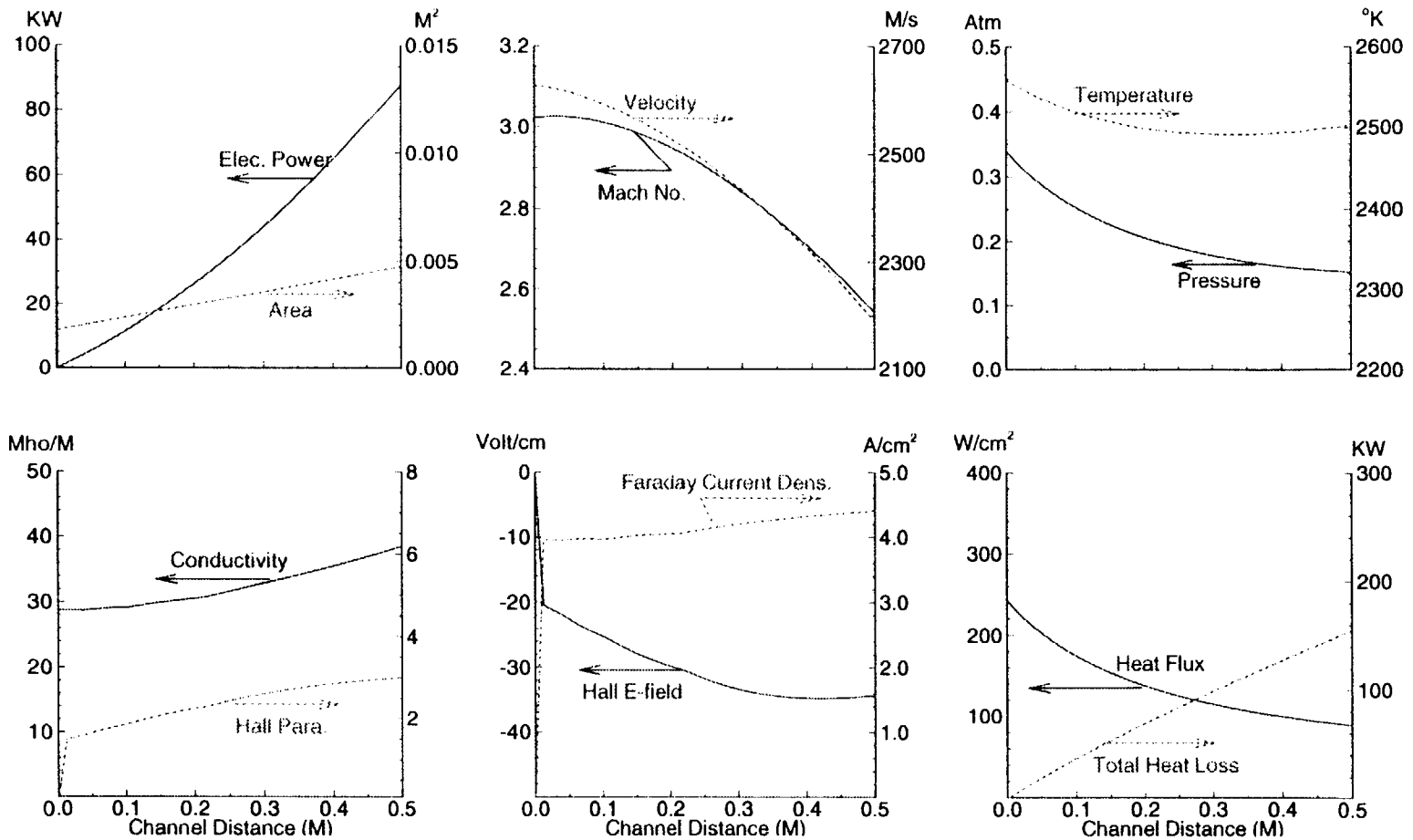

Figure 13 Calculated Flow and Electrical Parameter Distributions for the Designed 4° Half Wall Angle Faraday Generator. RP1 + O2 + CsOH, Cs(wt.%) = 9.66, $P_{comb.}$ = 300 psi, B = 1.5 T, Mass Flow = 0.235 Kg/s, $A_{MHD,inlet}/A_{throat}$ = 9.82, Channel Length = 20 inches (Equilibrium Flow Assumption).

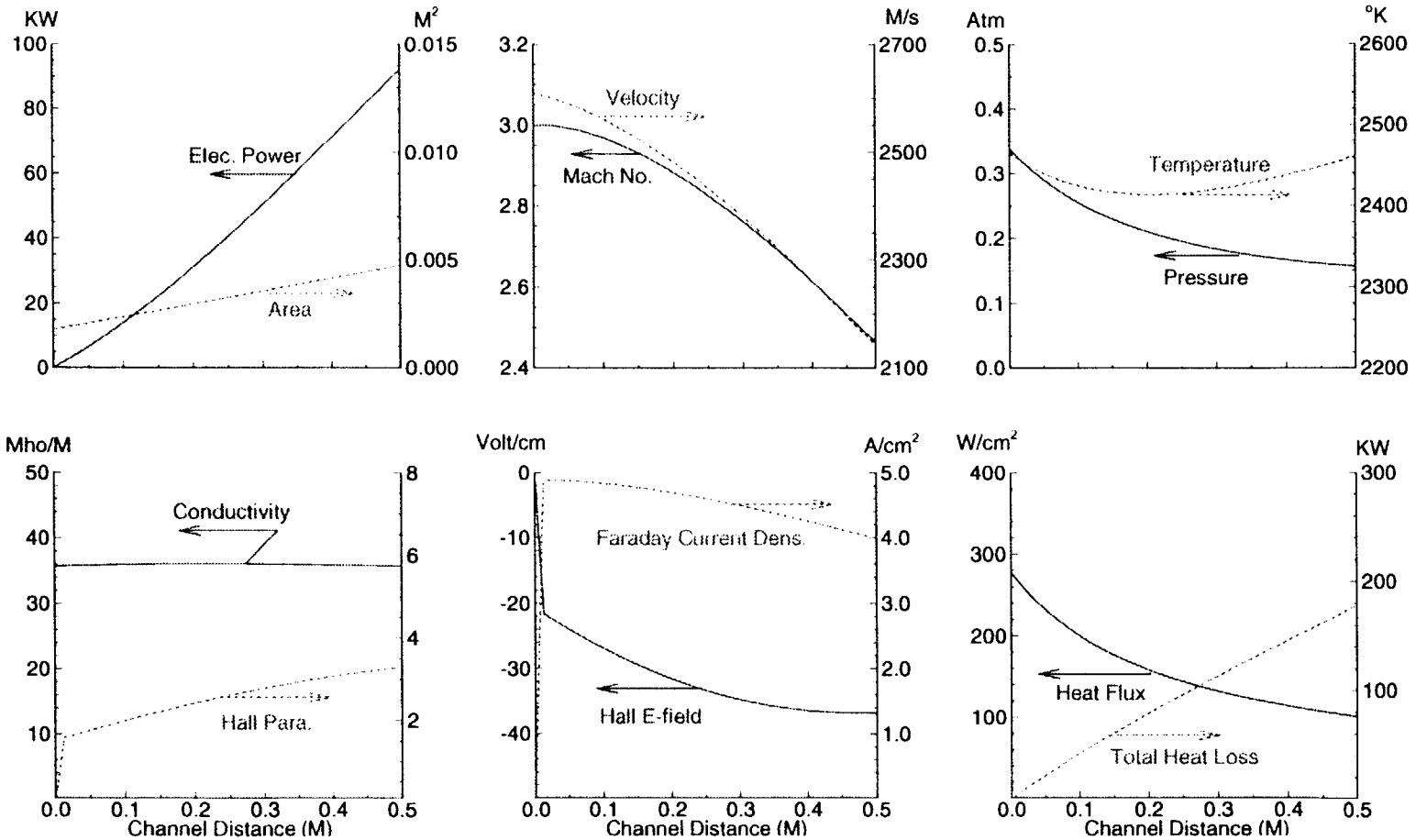

Figure 14 Calculated Flow and Electrical Parameter Distributions for the Designed 4° Half Wall Angle Faraday Generator. RP1 + O2 + CsOH, Cs(wt.%) = 9.66, $P_{comb.}$ = 300 psi, B = 1.5 T, Mass Flow = 0.235 Kg/s, $A_{MHD,inlet}/A_{throat}$ = 9.82, Channel Length = 20 inches (Frozen Flow Assumption).

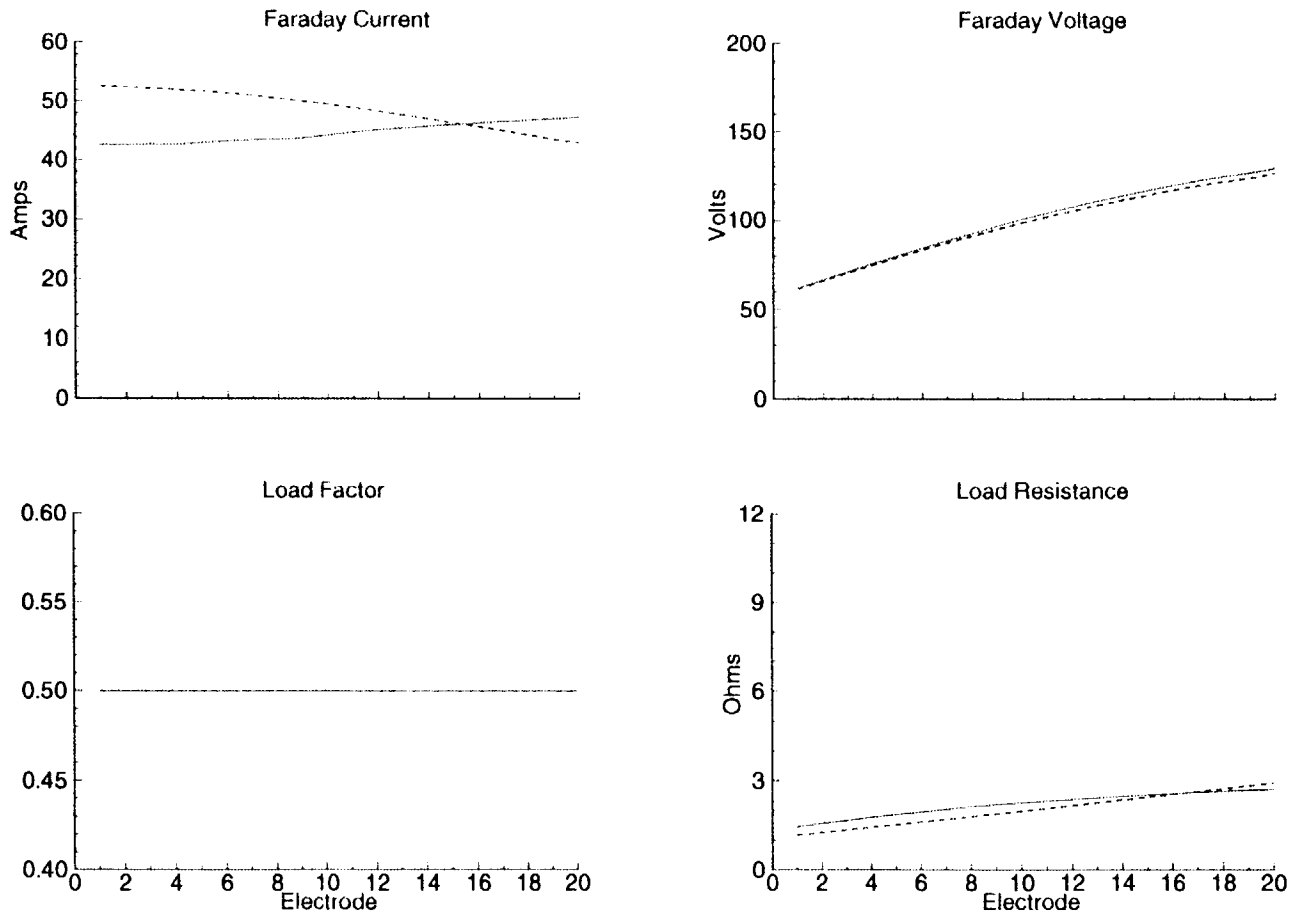

Figure 15 Loading Conditions for the Designed 4° Half Wall Angle Faraday Generator Using Cesium Seed.
(Solid Lines: Equilibrium Flow, Dashed Lines: Frozen Flow)

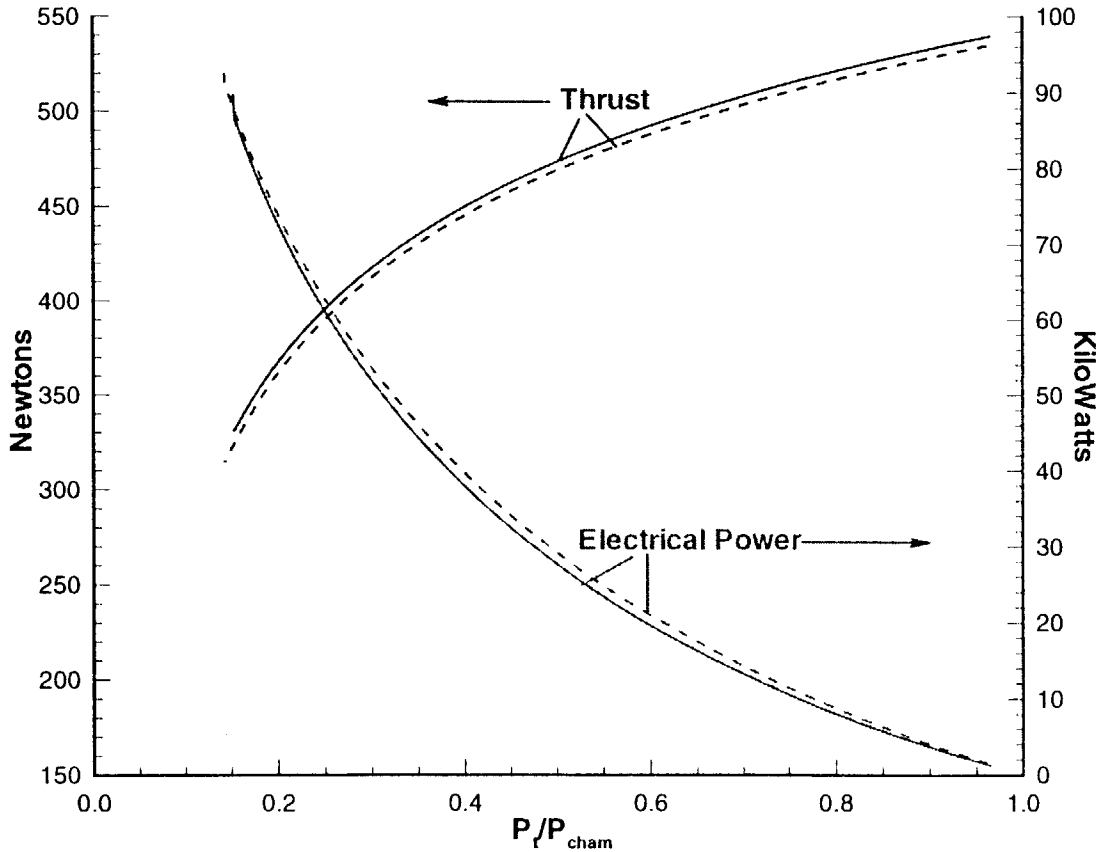

Figure 16 Relation between Thrust, Electrical Power, and Total Pressure Loss in the Channel of the Designed Rocket Driven MHD Generator Using Cesium Seed. (Solid Lines: Equilibrium Flow, Dashed Lines: Frozen Flow)

4. CONCEPTUAL MHD CHANNEL DESIGN

Because of the limited scope of the proposed testing program and because it is necessary to limit the development costs of the MHD channel, we based our conceptual MHD channel design on a heat sink configuration. Maximum operating times are not planned to exceed 10 to 15 sec. The detailed design strategy is based on practical experience with similar heat-sink configurations.

A schematic of the proposed electrode wall assembly for the Faraday channel is given in Fig. 17. This concept utilizes a phenolic back wall for insetting the electrodes and inter-electrode insulators. Phenolic is a plastic material which displays good electrical insulation characteristics and reasonably good high temperature resilience. The copper electrodes are attached to the back wall using standard fasteners. In addition, the electrodes are machined to accept thin aluminum oxide insulators. The recessed cuts on the electrodes holds the insulators in place, and the grooves are grouted with aluminum oxide filler.

The insulating sidewall also uses a phenolic back wall for insetting thermal and electrical insulating material. We propose to use aluminum oxide blocks or aluminum oxide casting material as the insulating material. The conceptual design for the sidewalls is shown in Fig. 18. This method has been proven to provide adequate thermal protection for short length tests.

The cross-section of the heat sink channel design, indicating the box wall construction method, is shown in Fig. 19. Note that the channel is based on a rectangular cross-section having an aspect ratio governed by the warm bore air gap of the magnet.

A schematic of the small-scale rocket based MHD system is shown in Fig. 20. Note that the modified rocket nozzle uses an adapter to change from a circular cross-section to a rectangular cross-section.

A schematic of the testing configuration for the small scale rocket based MHD system is shown in Fig. 21. This diagram indicates the propellant feed systems, auxiliary power systems, and measurement and control systems needed to test the rocket based MHD concepts.

Electrode Wall Assembly

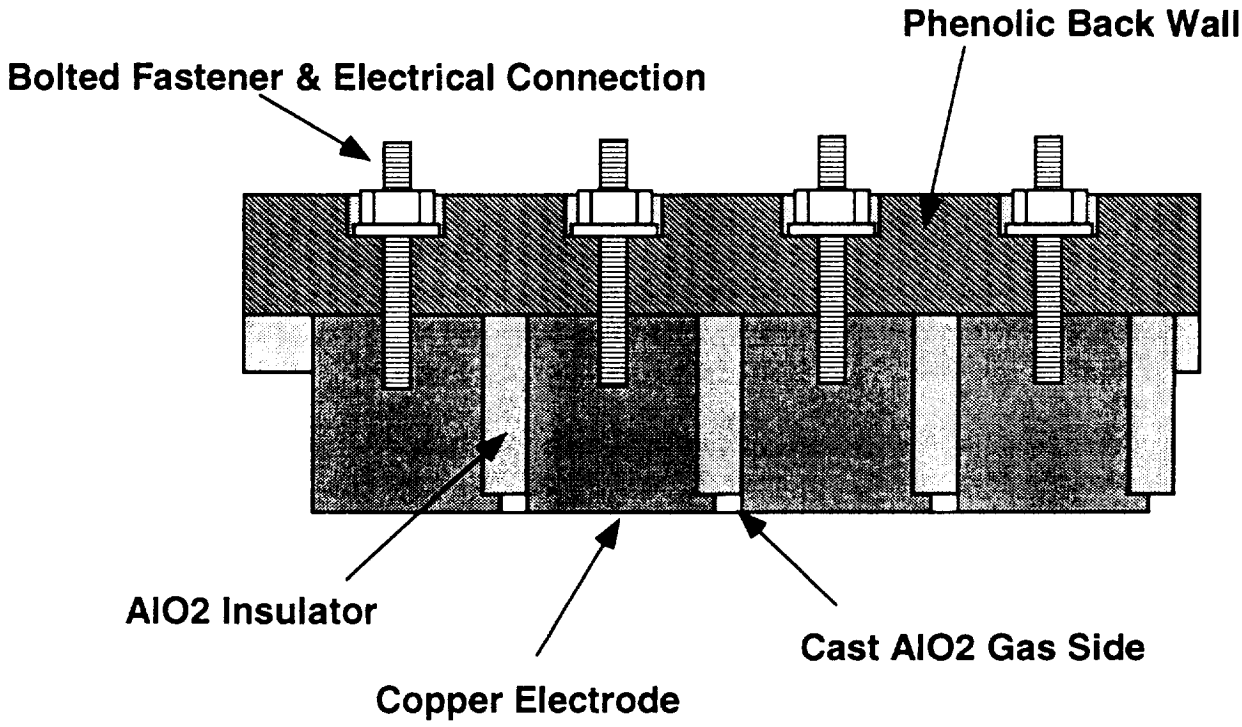

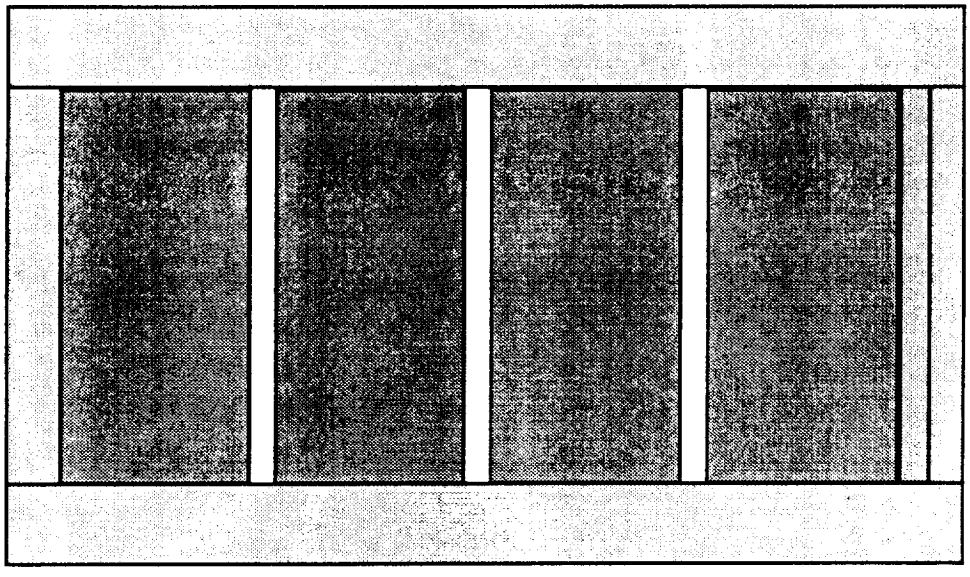

Figure 17 Conceptual Design of Electrode Wall Assembly for Faraday Channel

INSULATING WALL

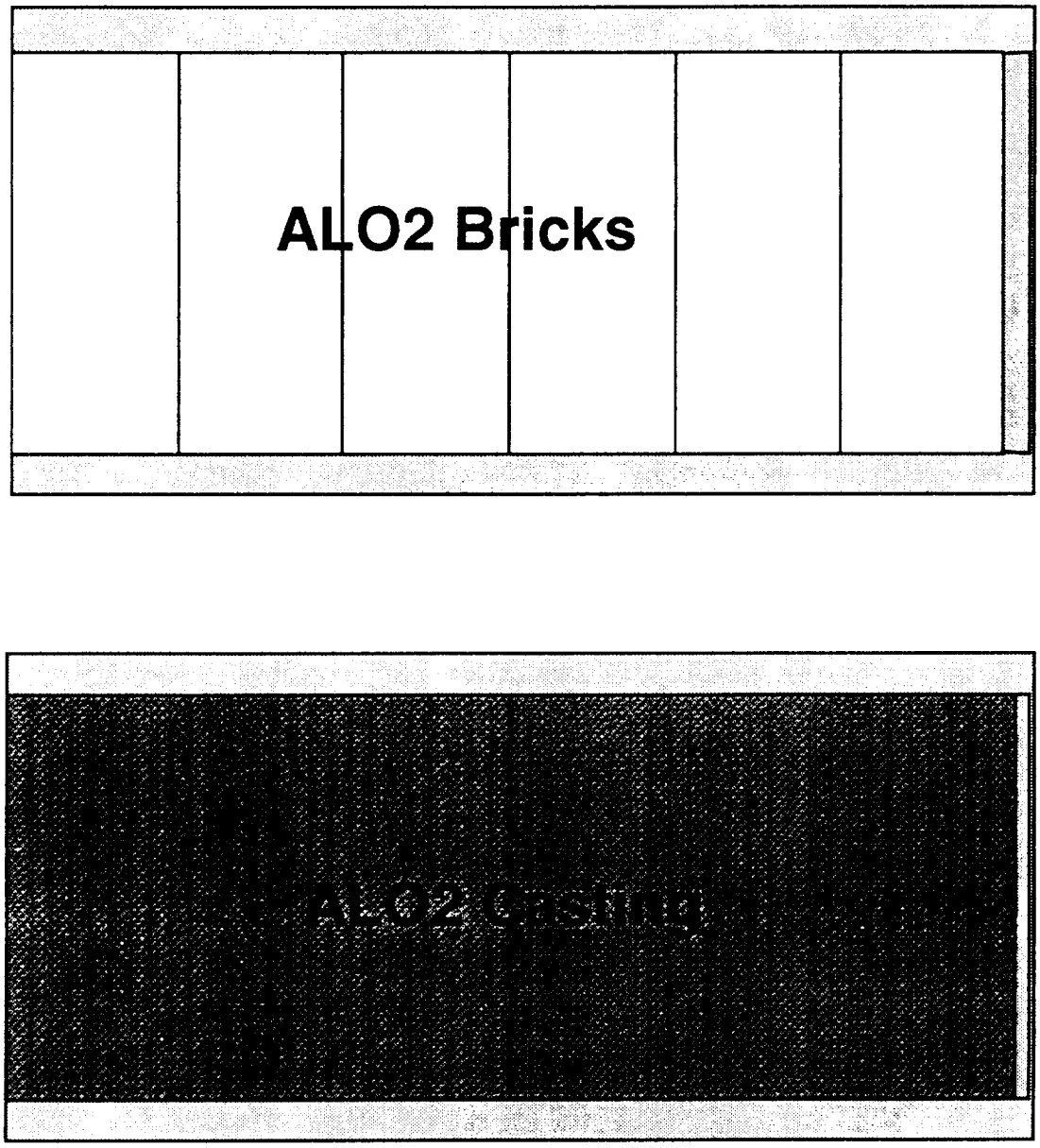

Figure 18 Conceptual Design of Insulating Sidewall Assembly for Faraday Channel

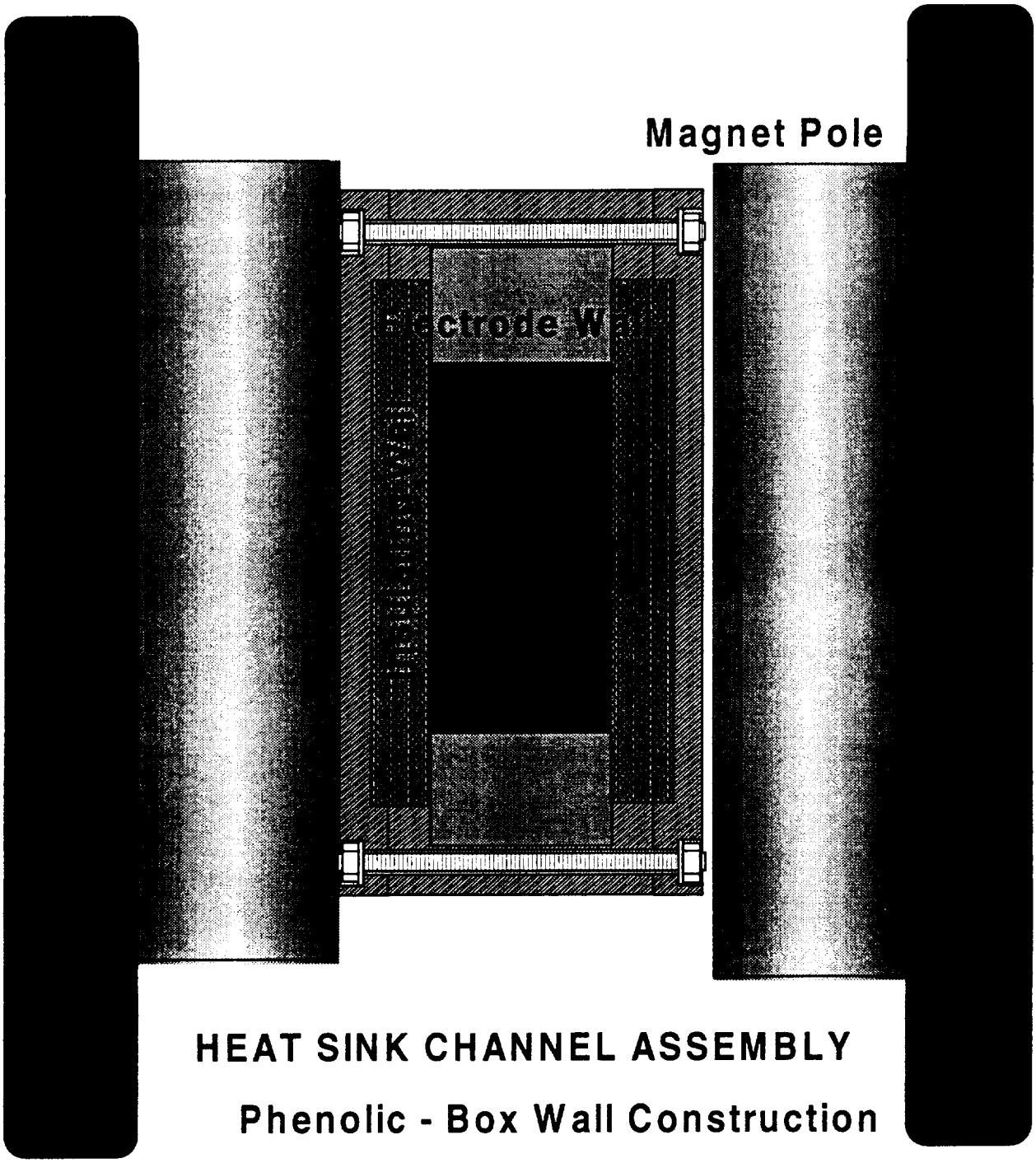

Figure 19 Conceptual Design of Heat Sink Faraday Channel Assembly

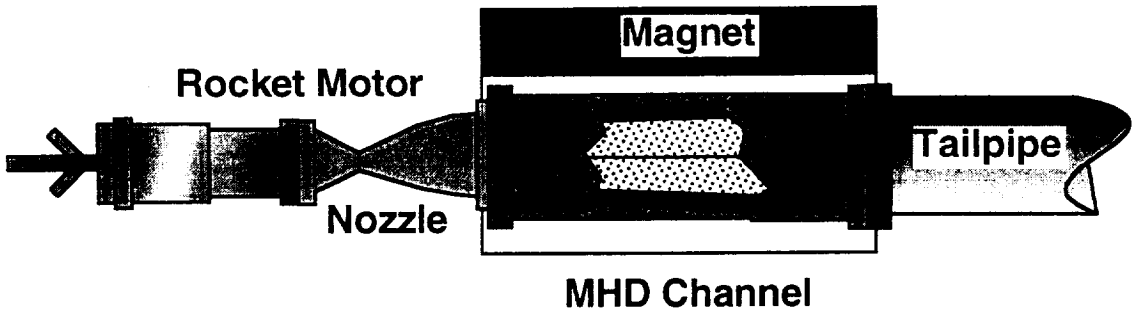

Figure 20 Schematic of Small-Scale Rocket Based MHD System

LIQUID ROCKET MHD GENERATOR TEST APPARATUS

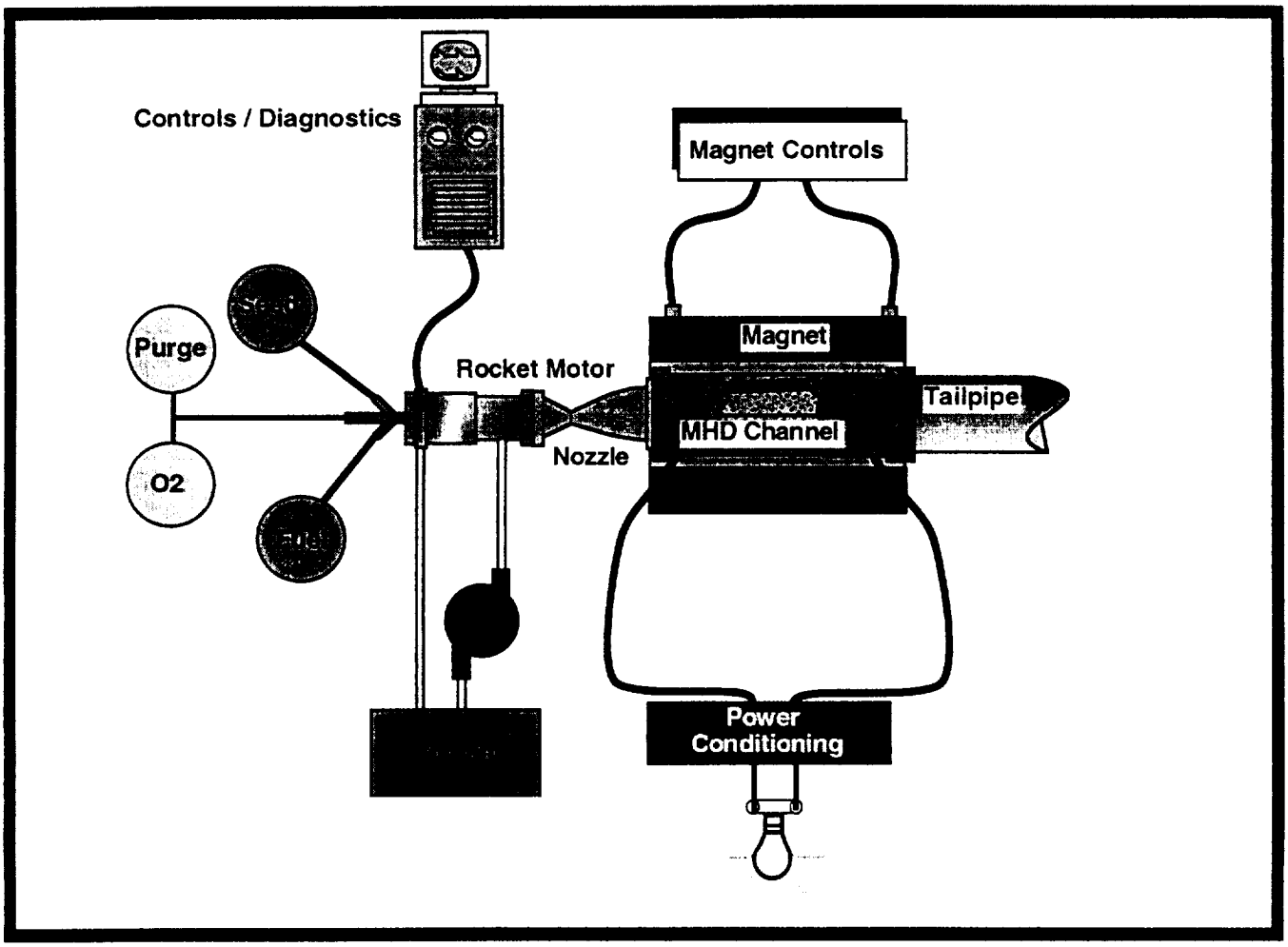

Figure 21 Schematic of Testing Configuration for Small-Scale Rocket Based MHD System

5. ROCKET BASED MHD ACCELERATOR

Detailed descriptions of the potentials of MHD accelerator technologies applied in hypersonic flight and sea water propulsion were given in References 15, 16, and 17, respectively. Following is a summary of the operation of an MHD accelerator and an estimate of performance potential of an MHD accelerator using operation conditions similar to that coupled to a rocket motor.

The MHD accelerator is composite system which consists of an MHD channel, a magnet, and a power supply as its major features. Operation of the accelerator consists of establishing the flow of a conducting fluid through the MHD channel, which is situated within a magnetic field directed normal to the flow. By application of an external power supply over the channel, an electrical current is forced across the conducting fluid. The action of Lorentz force on the fluid will then accelerate it, this action is manifested in the form of an increase in fluid total pressure. With the MHD accelerator channel designed for proper flow expansion through its length, the total pressure increase is in the form of velocity, or alternatively, flow kinetic energy. Joulean heat dissipation increases the total enthalpy of the flow. That is, within the MHD accelerator, simultaneous increase in flow total enthalpy and total pressure occur through the effects of Lorentz force as well as Joule heating. It is this fact which is often quoted when referring to the benefits of MHD flow acceleration over other heating technologies. Direct heating a channel flow increases the total enthalpy of the flow but, on the other hand, reduces the total pressure. The latter represents a loss to the effectiveness of the acceleration process.

The ideal Faraday accelerator is conceptually one with infinitely electrode segmentation such that no Hall current is present in the plasma. As a result, the Lorentz force is aligned with the flow direction and no side forces resulted. This is the type of MHD accelerator examined in this study since creation of uncontrollable side forces in the flow is generally unfavorable during the maneuver a rocket based system. Formulation of electrodynamics in the channel of a Faraday accelerator can be easily derived based on Ohm's law as

axial current $$j_x = 0 \tag{5}$$

Faraday current $$j_y = \sigma u B (K-1) \tag{6}$$

axial field $$E_x = \omega\tau u B (K-1) \tag{7}$$

Faraday field $$E_y = K u B \tag{8}$$

where the fields and currents are taken as integrated averages over the cross section, and K is the normal power supply load factor defined as

$$K = \frac{V_{applied}}{V_{open-circuit}} = \frac{E_y}{u B}, \qquad K \geq 1 \tag{9}$$

For a Faraday accelerator, the electrical efficiency can be written in terms of fundamental plasma variables by substitution in Equation (9). That is,

$$\eta = \frac{1}{K} \tag{10}$$

The expression (10) for the electrical efficiency shows that the most efficient Faraday accelerator is one operated with low load factor.

The Lorentz force and power supplied terms are then written as

$$\vec{u} \cdot (\vec{J} \times \vec{B}) = \sigma u^2 \ B^2 \ (K-1) \tag{11}$$

$$\vec{J} \cdot \vec{E} = j_y E_y = \sigma u^2 \ B^2 \ K \ (K-1) \tag{12}$$

The above expressions emphasize the need to maximize both the magnetic field and conductivity to enhance MHD interaction. The general performance of an ideal Faraday accelerator with a conductivity of 30 Siemens/m is depicted by the plots of Figure 22. These graphs illustrate the thrust current, electrical field, input power required, and push work produced for lines of constant induced electrical field ($\vec{u} \times \vec{B}$). For any given velocity and magnetic field combination within the range shown, the power density requirement can be estimated.

For example, for a rocket based MHD accelerator operating at a load factor of 1.1 (η = 90%) with a global plasma conductivity of 30 Siemens/m, velocity of 2500 m/s and a magnetic field of 2 Tesla (uB = 5 kV/m). At this condition, the ideal performance (no flow field losses) of the accelerator found from Figure 22 is current density 1.7 Amps/cm^2, applied field needed is 5.6 kV/m, 93 MW of electrical power for every is required, and 83 MW of MHD work per cubic meter of volume is produced to accelerate the plasma flow. Increasing magnetic field for the same operating point (moving to higher $\vec{u} \times \vec{B}$ lines) increases efficiency. At any given $\vec{u} \times \vec{B}$ value, higher power supplied or current density, leads to lower efficiency. As a result, to maximize efficiency over a specified speed range, low current and high magnet field are required.

The effects of increasing conductivity are shown in Figure 23 where increasing conductivity, for the same $\vec{u} \times \vec{B}$ value, decreases power requirement, promotes push power and leads to more efficient operation.

In consideration of a constraint on current density of 5 Amps/cm^2 as proposed in the generator design, the efficiency obtained from Figure 22 has to be no less than 75, 86, and 90% when uB has values of 5, 10, and 15 KV/m, respectively. Under such circumstances, the upper limits of the push power density are relatively 250, 431, and 750 MW/m^3 for uB of 5, 10, and 15 KV/m, while the corresponding limits on the required power are 333, 501, and 833, respectively.

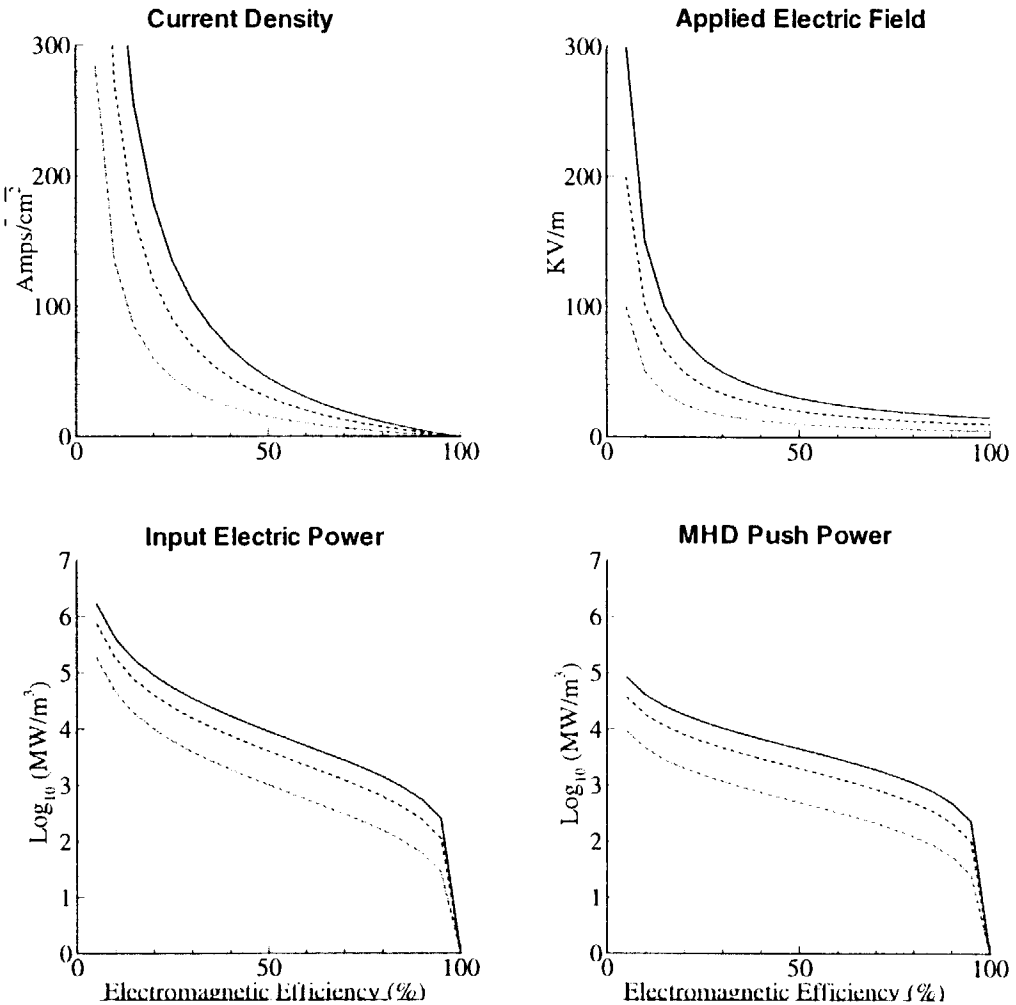

Figure 22 Performance Diagram for Ideal Faraday MHD Accelerator with a Conductivity of 30 Siemens/m (Solid Lines: uB = 15 kV/m, Dashed Lines: uB = 10 kV/m, Dash-Dotted Lines: uB = 5 kV/m)

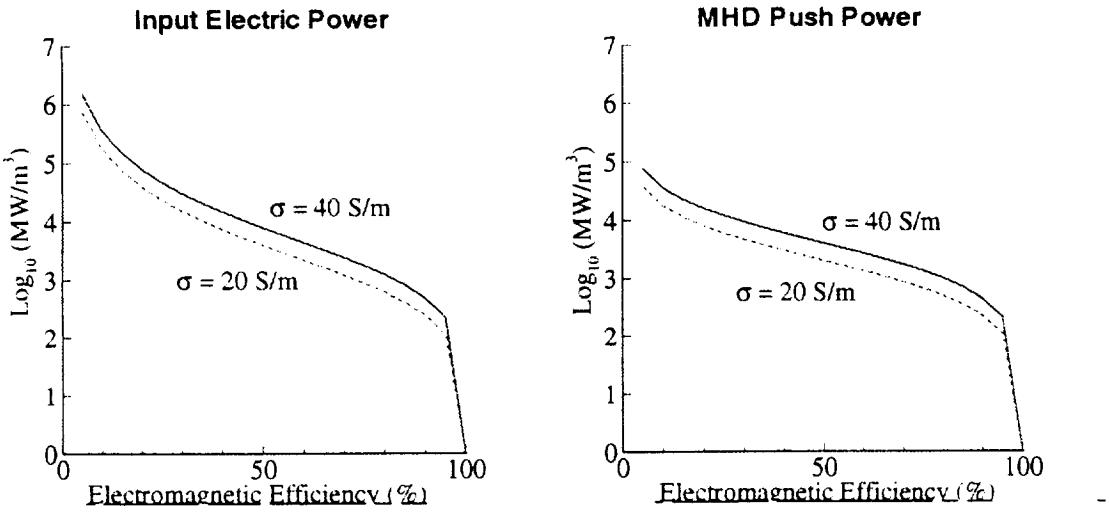

Figure 23 Comparison of Performance for Ideal Faraday Accelerator with Different Conductivities

6. CONCLUSIONS AND RECOMMENDATIONS

A Faraday type of MHD generator driven by a sub-scale LOx/RP rocket motor is conceptually designed based on an existing magnet and by assuming realistic limits on (1) the axial electric field, (2) the Hall parameter, and (3) current density, and (4) heat flux (given the criteria of heat sink operation). A parametric study is performed using GEN-1D computer code to find the optimum geometry of the MHD channel which not only satisfies all the specified constraints but also maximizes the electrical power. This study leads to a constant width MHD channel with a diverging half wall angle of 4 degree based on a combustion pressure of 300 psi. With a magnetic field of 1.5 Tesla, the electrical power output from this generator channel is estimated to be 54.2 KW with potassium seed and 92 KW with cesium seed. The parametric study shows that cases with 1000 psi combustion pressure can not simultaneously fit in the existing magnet structure and satisfy the designated heat flux constraint.

A conceptual design of the Faraday MHD channel and a testing configuration for the entire sub-scale rocket based MHD system are proposed. This Faraday Channel utilizes a phenolic back wall for inserting the electrodes and inter-electrode insulators. Copper electrode and aluminum oxide insulator are suggested for this channel. The thickness of the insulator wall is determined for a maximum operating time of 10 to 15 seconds.

The present design study is totally based on the ECF magnet and assumes that it can be refurbished to produce a magnet field strength of 1.5 Tesla. To fit into the narrow gap of this existing magnet, results of the parametric study show that the MHD channel must have a rectangular cross section to provide the required mass flow rate and to leave enough allowance for the wall thickness required for heat sink operation. A transition nozzle from circular to

rectangular cross section is thus needed to connect the rocket combustor and the MHD channel. Therefore, in addition to using this low cost magnet, it might be worthy, at the same time, searching for other candidate magnets which can provide higher magnetic strength, enough space for the MHD channel expansion, and consideration of employing a channel with circular cross section. Matching the circular rocket combustor with a circular MHD channel will result in a channel design much easier to be fabricated.

In this study, chemical non-equilibrium effects in high speed flow are accounted for by including certain degree of frozen flow effects to a chemically equilibrium model. To more precisely predict the influence of the non-equilibrium effects, modeling work including kinetics of different reactions should be developed. Also, multiple dimensional model is needed for better estimate of the boundary layer effects and the side forces effects in the MHD channels other than Faraday types.

It is strongly recommended to continue the rocket based MHD generator research program to testing phase in order to demonstrate power production from the designed generator, to set up a data base for verification of analytical modeling work, and to accumulate experience in designing and operating an MHD generator of this kind. Once these goals are reached, large scale rocket based MHD generators can be later designed to provide great performance with confidence.

Performance of a rocket based MHD accelerator is estimated without consideration of flow field losses. In this simple approach, current density, push power density, applied electrical field, and input power density can be found when conductivity, loading factor (or efficiency), and induced electrical field $\vec{u} \times \vec{B}$ are assigned. The results show that the lower the MHD interaction, the higher the efficiency in an accelerator. Higher conductivity decreases power requirement, promotes push power, and leads to more efficient operation. It is also found that with a current density constraint of 5 Amps/cm^2 and a conductivity of 30 Siemens/m, the push power density can be 250, 431, and 750 MW/m^3 when the induced voltage uB have values of 5, 10, and 15 KV/m, respectively.

More thorough analytical modeling of this rocket based MHD accelerator system taking into consideration of flow field losses is deemed absolutely necessary to better estimate the performance potential of this type of MHD accelerator under other practical constraints.

7. REFERENCES

1. Huth, J.H., "A Brief Study of Rocket Powered Magnetohydrodynamic Generators and Energy Storage Devices", The Rand Corporation, ARPA Order No. 91-59, May 1960.
2. Brogan, T.R., and Kantrowitz, A.R., "Very High Power. Limited Duty Cycle Rocket Driven MHD Generators", AVCO Everett Res. Lab. Rept. AMP 132, 1963.
3. Krzycki, L.J., Larsen, H.M., and Byrne, W.M., "Magnetohydrodynamic Power Generation from a Supersonic Rocket Exhaust", AIAA 5th Biennial Gas Dynamics Symposium, Northwestern University, Aug. 1963.
4. Berner, F., "MHD Turborocket Engine for Recoverable Launch Vehicles", AVCO Everett Res. Lab. Rept. 206, March 1965.
5. Maxwell, C.D., and Demetriades, S.T., "Feasibility Assessment for Space-Based Multi-Megawatt MHD System: Preliminary Conceptual Design.", STD Res. Corp. Rept. STDR-87-9(J), Feb. 1988.
6. Solbes, A., Weede, J., Hession, R., and Mitchell, P., "Design of a Ten Megawatt Rocket Driven Disk MHD Generator", 24th Intersociety Energy Conversion Engineering Conference, Vol. 2, p. 1073, Washington D.C., Aug. 1989.
7. Schulz, R.J. and Chapman, J.N., "Optimum Performance of MHD-Augmented Chemical Rocket Thrusters for Space Propulsion Applications,' ," 33rd Symp. on Engineering Aspects of MHD, Tullahoma, TN, June 1995, p.X.1 (Late Paper).
8. Myrabo, L.N., "Energy Beam Highways Through The Skies," MARIAH Workshop, Butte, MT, Nov. 1995.
9. Schmidt, H.J., Lineberry, J.T., and Chapman, J.N., "An Innovative Demonstration of High Power Density in a Compact MHD Generator", Final Rept., Contract No. DE-AC22-87PC79678, UTSI, June 1990.
10. Cole, J., Campbell, J, and Robertson, A., "Rocket-Induced MHD Ejector - A Single-Stage-to-Orbit Advanced Propulsion Concept", AIAA-95-4079, AIAA 1995 Space Programs and Technologies Conference, Huntsville, AL, Sep. 1995.
11. Wu, Y.C.L., et al., "Investigation of Diagonal Conducting Wall Generator", 13th Symposium on the Engineering Aspects of MHD, II.5.1, Stanford University, March 1973.
12. Gordon, S. and McBride, B.J., "Computer Program for Calculations of Complex Chemical Equilibrium Compositions", NASA-SP-273, 1971.
13. Frost, L.S., "Conductivity of Seeded Atmospheric Pressure Plasma", Journal of Applied Physics, Vol. 32, No. 10, Oct. 1961.
14. Wu, Y.C.L., "Performance Theory of Diagonal Conducting Wall MHD Generator", AIAA Journal, Vol. 14, No. 10, Oct. 1976, p.1362.
15. Lineberry, J.T. and Crawford, R.A., "The MHD Accelerator", Mechanical Engineering, Vol. 113, No. 9, Sep. 1991, p.70.

16. Lineberry, J.T. and Wu, Y.C.L., "Criteria for MHD Sea Water Propulsion", 25th Intersociety Energy Conversion Engineering Conference, Vol. 2, p. 546, Reno, NV, Aug. 1990.

17. Lineberry, J.T. and Chapman, J., "MHD Accelerators for Hypersonic Applications", AIAA-91-0384, 29th Aerospace Sciences Meeting, Reno, NV, Jan. 1991.

APPENDIX A

REVIEW OF RUSSIAN WORKS

ROCKET BASED MHD TECHNOLOGY

Prof. Valentin Bityurin

As part of this Task 1, ERC consigned its Russian consultant, Professor Valentin Bityurin to provide a synopsis on past and current Russian technology related to rocket based MHD concepts.

This Appendix presents the results of that background study.

MHD GENERATORS BUILT-IN IN ROCKET ENGINES. STATUS AND PROSPECTIVE

(Review of Russian Works)

ABSTRACT

In this report scientific information on R&D works available from open literature of Russian specialists on MHD built-in the of a rocket nozzle engine are present. It seems that the pick of activity in this field is passed 5-10 yeas ago for very clear reasons. It should be noted also that experimental investigations made are mostly occurred out of publications.

INTRODUCTION

Much attention has recently been given to the concept of all-electric aircraft [1,2]. To improve the tactical and technical characteristics of such vehicles, it is proposed to equip them with novel electrical and power facilities. Atmospheric vehicles with gas-turbine propulsion units utilising relatively low-temperature flows of a working medium ($T \leq 2000K$) are preferably provided with high-power electric sources such as electromechanical (in particular, synchronous) generators driven by the main propulsion units of the aircraft [3,4]. From the other hand it appears promising to equip aerospace vehicles with high-temperature ($T \geq 3000K$) rocket engines with MHD generators (MHDG) used as high-power airborne power sources [5-7]. The use of MHDG in the power facilities will make it possible to produce new types of electrical jet engines for aircraft, replace the conventional turbopump units in liquid-propellant rocket engines by advanced fuel supply systems, and accomplish the MHD control of the thrust vector at aerospace vehicles [8-12]. An MHD generator installed in this nozzle of a scramjet is considered as a one of the main component of an deep optimized thrust system of hypersonic transatmospheric aircraft [12].

Research and development works in field of interplanet voyages and, in particular, a manned mission to the Mars considers a nuclear power production/thruster facility based on a nuclear gas-phase reactor with magnetic stabilization of active material as one of the most prospective solution [13,15]. For such an on-board power generating facility the MHD generator located somewhere in nozzle of the nuclear rocket engine could be a rather effective electricity generating unit [15,16].

In the most papers devoted to airborne high-power MHD generators (self-contained or built into the nozzle of the propulsion unit), MHD channels are discussed that are based on a two-pole scheme. The processes of energy conversion in these MHD generators are usually accompanied by disturbances of flow in the entire channel volume. Being an auxiliary power generating most built-in MHD generator should be a low disturbing device that does not decrease significantly the overall performance of the power generating system. For this reason the MHD generator working volume should presumably occupy only small portion of the whole working volume of the power facility. One of the approach helping to solve this problem is an utilization a multipolar magnetic system instead of the traditional two-pole system. Depending on the number of pairs of poles, the proposed facility makes it possible to accomplish MHD conversion both in the nozzle peripheral zone and in the central part of the flow.

SCHEMES OF MULTIPOLAR MHDG

In the multipolar MHD generators under consideration [6,7], the electrodes may occupy a part of the surface of thin cylindrical rods (Figs.1a and 1b) or be installed on U-shaped projections (Fig.1c) and on the side walls of the channel (Fig.1d) [6,7]. The magnetic field **B** is produced by a multipolar magnet system (MS), which consists of $2P$ current-carrying linear sections located above the electrodes. With $P \geq 2$, such a magnet system has low scattering fields as compared to the traditional magnet system, and this is important for the airborne multipolar MHDG. The current-conducting gas moving with velocity v and interacting with the magnetic field causes electric current in the load. The external wiring of the electrodes of a multipolar DC MHD generator and the definition of basic geometric parameters of MHD channel having modules of different are shown in Fig.1.

In the other versions electrodes are set on the U-shape projections (Fig.1.d) or on the cilindrical channel walls (Fig.1.e). The external magnetic field **B** is formed by a multipolar magnetic system containing 2P linear sections with the transverse dimensions $r_M << r_0$. Outside the channel the sections are located on radius $r_M > r_0$ directly above the electrodes. Fig.1.f shows the external electrode commutation for DC and one-phase AC generators. It is also possible to get a three-phase AC from MHDG if the magnetic system is excited by a three-phase AC and another versions of the electrodes commutation is used.

Further it assumed anways that the magnetic fields induced by the electric currents in MHD channel can by neglected. The period of AC is much more than the period of the gas flight through the channel. The length of MHDG L is considered to be much large than the distance between the electrodes. The end effects in channel are rather small. The supersonic and subsonic flow regimes at the finite values of Hall parameter ($\beta_0 \neq 0$) and high hydrodynamic Reynolds numbers (Re>>1) are studied. This allows to describe three-dimensional processes in the channel usual MHD approximations for a stationary nonviscous ideal gas flow [17,19]. (Additionally the influence of the thin boundary layers is taken into account when the electrodynamic problem is further discussed.). The dimensionless MHD equations are the following:

$$\mathrm{div}(\rho \mathbf{u}_\cdot)=0: \qquad (1)$$

$$\rho_\cdot(\mathbf{u}_\cdot \mathrm{grad})\mathbf{u}_\cdot=-(1/(\gamma M)^2)\mathrm{grad}\,\rho_\cdot+S/\lambda \mathbf{J}\cdot\mathbf{B}: \qquad (2)$$

$$\rho_\cdot T_\cdot(\mathbf{u}_\cdot \mathrm{grad})s_\cdot=SM^2\gamma(\gamma-1)\mathbf{J}_\cdot^2/(\lambda\sigma_\cdot): \qquad (3)$$

$$\mathbf{J}_\cdot+(\beta_0/|\mathbf{B}|)\mathbf{J}_\cdot\times\mathbf{B}=\sigma_\cdot(\mathbf{u}_\cdot\times\mathbf{B}_\cdot+\mathbf{E}_\cdot): \qquad (4)$$

$$\mathrm{div}\,\mathbf{J}=0: \quad \mathbf{E}_\cdot=-\mathrm{grad}\,U_\cdot: \qquad (5),(6)$$

$$\mathrm{div}\,\mathbf{B}_\cdot=0: \quad \mathrm{rot}\,\mathbf{B}_\cdot=0 \qquad (7),(8)$$

$$p_\cdot=p_\cdot T_\cdot: \quad s=\ln(p_\cdot/\rho_\cdot^\gamma): \quad \sigma_\cdot=\sigma_\cdot(p_\cdot,T_\cdot): \quad \beta_0=\beta_{e0}(p_\cdot,T_\cdot)|\mathbf{B}|; \quad u_\cdot=u_\cdot/u_0:$$

$$T_\cdot=T_\cdot/T_0: \quad p_\cdot=p_\cdot/p_0: \quad \rho_\cdot=\rho_0/\rho_0: \quad \sigma_\cdot=\sigma_0/\sigma_0: \quad \mathbf{E}_\cdot=\mathbf{E}_\cdot/(u_0B_0):$$

$$\mathbf{J}_\cdot=\mathbf{J}_\cdot/(\sigma_3 u_0 B_0): \quad B=B_\cdot/B_0.$$

Here the inferior index «*d*» corresponds to dimensional values: «0» — to base values at the inlet of MHDG; «*» — to dimensional values: u $\{u_\cdot,u_\cdot,u_\cdot\}$ is a gas velocity: ρ, p, T and s are a density, pressure, temperature and gas entropy respectively: $\sigma_\beta=\sigma_0/\left(1+\beta_{eo}^2\right)$ is an effective plasma conductivity: **J**, **E** and U are an electric current density, electric field and electric potential respectively: $M=u_0/\sqrt{\gamma R T_0}$ and $S=\sigma_{\beta 0}B_0^2/(\rho_0 u_0)$ are Mach number a parameter of MHD interaction: γ, R are an adiabatic coefficient and gas constant: $\lambda=L/r_0$ is a relative channel length:

$B_0 = \mu_0 I_{M0} n_0^{p-1} / (\pi \rho_m^p)$ is a characteristic value of the magnetic flux density ($\mu_0 = 4\pi \times 10^{-7}$); $I_{M0} = pI_p$ is the total current through p sections of MS.

At a weak MHD interaction (S<<1) the problem is solved by means of perturbation techniques, when dependent variables, such as u_*, p_*, T and etc., are presented as the asymptotic expansion series:

$$u_* = u + S \cdot u_s + \varepsilon_0 \cdot u_0 + \ldots; \quad p_* = p + S \cdot p_s + \varepsilon_0 \cdot p_0 + \ldots \tag{9}$$

Here S<<1 and $\varepsilon = r_c / r_0 << 1$ are small parameters; the values without index belong to zero-order approximation; lower «*s*» and «*e*» indexes correspond to the first approximation of perturbanced parameters according to s and ε respectively. At $s<<1$ the unperturbanced gasdynamic parameters in MHDG are known. With this assumption the values **B** and **J** can be found from the independent solution of two elliptic problems Eq (4)-(6) and Eq (7)-(8).

For long cylindrical MHD channels ($\lambda = L/r_0 > 4$ to 5, see Fig.1) the distribution of **B** and **J** away from the end zones is found from the independent solution of two elliptic problems of the form [19]

$$\begin{cases} \Delta A_z = 0 \\ \mathbf{B} = \mathrm{rot}(A_z \mathbf{i}_z) \end{cases} \qquad \begin{cases} \Delta_{r\varphi}\Psi + \Delta_{r\varphi} \ln\left[\sigma/(1+\beta^2)\right] \nabla_{r\varphi}\Psi = 0 \\ \mathbf{J} = \sigma\left[\nabla_{r\varphi}\Psi + \mathbf{i}_z \beta \left|\nabla_{r\varphi}\Psi\right|\right] / (1+\beta^2) \end{cases} \tag{10}$$

where $\mathbf{A}(0,0,A_z)$ and $\Psi = \mathbf{vA} - U$ are the vector potential of the magnetic field and the electric current density potential, respectively; U is the electric field potential in the MHD channel; σ and v are the electrical conductivity and velocity of gas, respectively.

After that one can find perturbanced fields of the corresponding gasdynamic values (u_s, p_s, ρ) from the corresponding solution for M>1 of the inhomogeneous hyperbolic problem of the form [19].

$$\begin{aligned} &\Delta_{r\varphi}\chi - (M^2-1)\partial^2\chi/\partial z^2 = f(\mathbf{J},\mathbf{B},\bar{r}) \\ &\mathbf{v}_s = -\mathrm{grad}_{r\varphi z}\,\chi + \int_0^z (\mathbf{J}\times\mathbf{B})dz \end{aligned} \tag{11}$$

where χ is the velocity disturbance potential $\mathbf{v}_s(v_r, v_\varphi, v_z)$; and $f(\mathbf{J},\mathbf{B},\bar{r})$ is the known function of $\mathbf{J},\mathbf{B},\bar{r}$, whose structure is determined by the design of the electrode modules (Fig.1).

At a high MHD interaction (s>0.5) the characteristics of MHDG with the variable cross-section are determined on the base of one-dimensional MHD equation [17,19].

The analytical solutions for the calculation of the parameters A_z, Ψ, χ of multipolar MHDG at s<<1 are given in [19]. Figures 2a and 2b show the calculation results of the typical distribution of the function of the magnetic flow A_z and current density potential Ψ in cylindrical MHDG with U-shaped electrodes. The function A_z=const is given for the case of P=3 and P=5. The isolines $\Psi[r,\varphi,k_1(1-k/k_{n1})]=\text{const}$ are constructed for P=3, the load parameter k=0.5 and the typical values of the short-circuit current drop factor k_1 and no-load voltage factor k_{n1} (the factors k_1 and k_{n1} allow for the effect of σ and ν on Ψ in the electrode boundary layer). Figure 2c also shows the distributions of the dimensionless velocity disturbances $\mathbf{v}_s(v_{sr}, v_{s\varphi}, v_{sz})$ in an MHDG with $\lambda=L_c/r_0$=3 for different Hall numbers (β=0 and β=1.72). The calculations of A_z, Ψ, and $\mathbf{v}_s$ were performed for the case of small cross-sectional size of the linear portions of the magnetic system. From Fig.2, it is clear that the distributions of A, Ψ, and v_s, at $P\geq 2$ are nonuniform in the channel cross section. The process of MHD energy conversion is localised in the peripheral zone. At β=0, the axial symmetry of the disturbance fields of the velocity v_s, is broken, and cross eddy currents are formed in the MHD channel outside of the flow. This effect results in deviation of disturbed flow to the cathode electrodes.

It is well known that ideal single-pole MHDG (P=1) with electrodes arranged on the channel side walls (as shown in Fig.1d) feature higher energy characteristics at a constant level of the magnetic flux in the interelectrode zone. However, their technical realisation in airborne power facilities has a number of disadvantages. These include the contraction of currents on the electrode edges, high scattering fields of the magnet system, high consumption of ionising seed, disturbances in the entire nozzle volume [19]. As mentioned above, multipolar MHDG with U-shaped electrodes are free from these disadvantages and provide diffusion current flow in the channel, low scattering fields and a low flow rate of the ionising seed in the zone of effective MHD-interaction [6].

The output parameters of multipolar MHDG with $s\leq 1$ in MHD channels that are barely expanding along their length can be estimated using quasi-one-dimensional dimensionless MHD-equations, averaged over the channel cross section, of the form [19]

$$\rho v_z F(z)\left(1-q(z)-\frac{\pi\delta^{**}}{r_0}\right)=1 \quad . \qquad (12)$$

$$\rho v_z \frac{dv_z}{dz}=-\frac{1}{\gamma M^2}\frac{dp}{dz}+s\frac{1}{\lambda}\langle \mathbf{J}\times\mathbf{B}\rangle_z+2\left(\frac{C_f}{D_f}+\frac{C_p}{D_p}\right)\rho v_z^2 \quad . \qquad (13)$$

$$\rho v_z \frac{d}{dz}\left(T+\frac{\gamma-1}{2}M^2 v^2\right)=sM^2(\gamma-1)\langle \mathbf{J}\cdot\mathbf{B}\rangle\frac{1}{\lambda}+2C_f\frac{\rho v_z}{D_f}(T_w-T_w) \quad . \qquad (14)$$

$$\frac{d\delta^{***}}{dz}+\frac{\delta^{***}}{\rho}\frac{d\rho}{dz}+(2+H)\frac{\delta^{***}}{v_z}\frac{dv_z}{dz}=\frac{C_f}{2} \quad .$$

$$p=\rho T \quad , \quad T_w=T+0.9\frac{\gamma-1}{2}M^2 v_z^2 \quad . \qquad (15)$$

$$r_0 s=\frac{\sigma_e B_0^2 L_0}{\rho_0 v_0} \quad , \quad \sigma_e=\frac{\sigma}{1+\beta^2} \quad .$$

Here, C_f and C_p are the coefficients of friction in the channel and of pressure loss on the electrode modules [20,21]: $D_f=4F/\Pi$ and $D_p=4FL/(2P\pi r_c^2)$ are the hydraulic diameters; q is the factor of shading of flow by the electrode modules; δ^* and δ^{**} denote the displacement and momentum thickness, respectively; γ is the adiabatic coefficient; $\lambda=L/r_0$ is the relative length of the MHD channel; ρ, p, T, and v_z are, respectively, the dimensionless density, pressure, temperature, and axial velocity of the gas flow; s and M are, respectively, the MHD-interaction parameter and the Mach number, determined by the gas parameters at the inlet; $H=\delta^*/\delta^{**}$ is the form parameter of the boundary layer; T_w is the channel wall temperature.

Within this approach, the friction coefficient C_f is determined on the basis of the limiting laws of friction and heat transfer [20]. The cross section-averaged specific electromagnetic $\langle \mathbf{J}\times\mathbf{B}\rangle_z$ and electric power $\langle \mathbf{J}\cdot\mathbf{E}\rangle$ in (12)-(15) are found from the solution of the two-dimensional electrodynamics problems on transverse edge effect in cylindrical multipolar MHD channels [19].

Figure 3 shows typical dependences of the values of $\langle \mathbf{J}\times\mathbf{B}\rangle_z$, $\langle \mathbf{J}\cdot\mathbf{E}\rangle$ short-circuit current I_{sc} and open-circuit voltage U_{oi} on the size r_c of electrode modules of MHD channels with U-shaped (Fig.3a) and segmented [Fig.3b, where $\delta=(\varphi_0-\varphi_1)/\varphi_0$] electrodes. The dots in Fig.3a indicate the results of the experimental study of the characteristics of

multipolar MHD channels [22]. Experimental data have been obtained for P=1.2.3 in plasma MHD-models with the channel length L_{ch}=1.75m and radius r_0=0.6m with the following parameters of argon flow: flow rate G~2g/s. Hall parameter β~1-2. effective conductivity in the core σ_e~50 to 100S. MHD-interaction parameter s~0.1 [22.23]. From Fig.3 it is clear that the experimental data agree with the theoretical dependences. and this fact enables one to recommend them for the calculation of concrete versions of propulsion units with a multipolar MHD generator.

For the given geometry of the engine nozzle and s<<1. the approximate analytical solutions of system (12)-(15) for the dimensional quantities of current I_{gen} and power N_{ren} of MHDG with U-shaped electrodes have the form [19]

$$I_{gen} = 2\pi P \int_0^{L_{ch}} \left\{ \sigma_e k_l \left(1 - \frac{k}{k_{nl}} \right) v \frac{\mu_0 I_0}{\pi} \left(\frac{r_0}{\rho_e} \right)^{\gamma} \frac{\mathrm{Pr}_e}{r_0} \left(1 - \frac{1}{2} \left(\frac{\mathrm{Pr}_e}{r_0} \right)^2 \right) \right\} dz \quad . \tag{16}$$

$$k(z) = U_0 k_{nl} \left\{ 4v(z) \frac{\mu_0 I_0}{\pi} \left(\frac{r_0}{\rho_e} \right)^{\gamma} \frac{\mathrm{Pr}_e}{r_0} \left(1 - \frac{1}{2} \left(\frac{\mathrm{Pr}_e}{r_0} \right)^2 \right) \right\}^{-1} \quad . \tag{17}$$

$$N = U I_{gen}(z) \quad .$$

$$\langle k \rangle = \frac{u}{u_{nl}} = \frac{k_{nl} \int \sigma dz}{\int \frac{\sigma}{k(z)} dz} \quad . \tag{18}$$

Here. U is the MHDG voltage: $k(z)$ is the local load factor: I_0 is the total current (magnetising force) of the magnet system section: $\mu_0 = 4\pi \times 10^{-7}$ is the magnetic permeability. The typical dimensions of the elements in the MHDG cross section are shown in Fig.1.

Relations (16)-(18) make it possible to calculate the output characteristics of the built-in multipolar MHDG at s<<1 and can be used for optimisation of the power facility parameters.

EXPERIMENTAL INVESTIGATIONS

Experimental facilities. The experimental investigations of multipole MHDG were carried out on the plasma-vacuum equipment [24]. Argon plasma parameters at the inlet of the experimental MHDG had the following values: velocity ~500÷2000m/sec; Mach number M~0.5÷2.0; gas temperature ~(8...12)×10³K; static pressure ~10³Pa; mass flow rate G~2÷5g/sec; average Hall parameter β~1÷2; average effective electrical conductivity σ_e~(2÷4)× 10³s/m; parameter of MHD interaction S~0.5÷1.0. Magnetic flux density in the channel was changed from 0.1 to 0.4T. In experiments (see Fig.4:) argon entered the heater (plasmatron) 1 and then came through the nozzle and MHD-channel 2 to the vacuum cavity 3. Fig.4 shows a general view of experimental DC multipole MHDG with a cylindrical channel with radius r_0=60mm. 2P electrodes 4 with length L_K=175mm are symmetrically located on radius ρ_e=46mm in the peripheral channel zone. The electrodes were made as thin graphite cylindrical bars by radius r_e=9mm. The external magnetic field in MHD channel was formed by multipole magnetic system (MS) 5.

MHD characteristics. Fig.5 shows the voltage current $U_p(I)$ and power $N_p(I)$ characteristics of MHD channel at the different pole number P=1,2,3. In the experiments we have an electrical current for MS I_{ms}=400A (B~0.3T), mass flow G_1≅2g/sec, gas velocity u_c=400-500m/sec. The dependencies $U_p(I)$ for multipole MHDG have the falling character. The value of the highest electrical power is obtained in the channel at P=2. It can be explained by the fact that at P=2 we have the greatest values of the magnetic flux density. Fig.5 also represents the comparison of dimensionless theoretical and the experimental data [6]. It's evident that the experimental data qualitatively correspond to theoretical curves.

DESIGN AND PARAMETERS OF PROPULSION UNIT WITH MHDG

Figure 6 illustrates a version of a propulsion unit with a multipolar, MHDG built in the nozzle of a liquid-propulsion rocket engine. The facility utilises cryogenic fuel components $H_{2l}+O_{2l}$. The readilyionizable cesium seed is fed directly into the wall zone of the nozzle. The relative flow rate of cesium $\gamma_C \sim G_C/G_\Sigma \sim 0.3/(P+1)$ (here, G_C and G_Σ are, respectively, the cesium and fuel flow rates in the propulsion unit) is selected so as to provide the required level of ionisation and conductivity in the annular zone Δ of the multipolar MHDG in the corresponding region of effective MHD interaction of the flow ($\Delta \sim r_0/(P+1)$) [19]. The body of U-shaped cooled electrode modules I of the MHDG is made of copper and faced with segments 2 of pyrographite on the side of high-temperature flow (see Fig.6). The internal copper-faced surface of the graphite segments is soldered to the copper body of the electrodes. The electric current from the electrode modules flows through tubular copper current conductors 3 insulated from the body and used for the delivery of the cooling agent (H_{2l}). From the external side of the propulsion unit nozzle, the electrodes of like polarity are alternately connected to cooled annular current conductors 4. In order to provide electric insulation, the hot walls of the nozzle 5 are separated from the electrodes by refractory spacers 6 made of concrete with a filler of the MgO type. In the interelectrode zone, the nozzle walls are covered with thin insulating modules based on Al_2O_3. Intensive cooling of the nozzle by the oxidizer (O_{2l}) provides additional protection against electric breakdown thanks to the formation of a cold wall boundary layer. The multipolar magnet system consists of $2P$ racetrack coils or sections 7. Each section is wound by reinforced wire of ultra-pure aluminium A_{9999} having a high electrical conductivity [23]. The sections can be cooled by liquid hydrogen through a system of longitudinal axial channels. The multipolar magnet system with power elements is mounted on the external wall of the nozzle in an airtight welded housing 8. To remove the power loads of the magnet system arising during the MHDG operation, the magnet system housing is additionally secured to the propulsion unit carrier frame. The bondage and rigidity of the winding and bandage elements of the magnet system were estimated using the methods described in [25].

The main parameters of the advanced power facility with a liquid-propulsion rocket engine and a built-in multipolar MHDG are given in the table. The properties of the products of combustion of the working medium $H_{2l}+O_{2l}$, with the air excess factor (α=0.8, seeded with alkali metal (cesium), and the specific performance of the liquid-propellant rocket engine were borrowed from [26,27]. The calculation of the output characteristics of the MHDG according to (16)-(18) was performed for the pairs of

poles of P=3.5. The coefficients of decrease of the short-circuit current k_i and the open circuit current k_{ni} were taken equal to 0.9 [19,29]. The load factor k=0.75. Given in the table are the results of the calculation of the parameters of a built-in MHDG for two values of the pairs of poles P=3 and P=5, whose magnet system is characterized by weak scattering fields in she far zone. The size of the electrode modules $\bar{r}_e=r_e/r_0$=0.05 is selected taking into account the fact that the loss of specific thrust of the propulsion unit due to the electrodes protruding into the flow is low compared to the losses due to MHD-processes in the propulsion unit nozzle ($r_e << r_0^4\sqrt{N\lambda^2/kGv^2PC_*}$, where $C_*\equiv 1$ [18]). The dependences of the output parameters for other values of r_e and P are given in Fig.7.

The analysis of the theoretical data obtained (see the table and Fig.7) has shown that the proposed version of the propulsion unit with a thrust P~80.0 ton and a multipolar MHDG makes it possible to obtain electrical power N~10MW with low losses of the thrust ($\Delta P/P \sim \Delta P_{sp}/P_{sp}$~0.005). With the same magnetizing force (total current) in the magnet system, an increase of P *at* $r_eP<0.5$ causes an increase of the useful generator power and a decrease of the size of the annular zone $\Delta_e \sim r_0/P$, where the disturbance of gas flow is appreciable. The power of a multipolar MHDG may be increased at $r_eP<0.5$ with the same composition of the combustion products by increasing the size of the electrode modules. In this case, however, the propulsion unit thrust losses will increase due to aerodynamic losses in the nozzle. The power of an MHDG utilizing the working medium $H_{2l}+O_{2l}$ with alkali seed may be increased by adding aluminium powder into the fuel, this increasing the combustion temperature and, therefore, the electrical conductivity of gas in the MHD channel [29].

The proposed scheme with a multipolar MHDG can also be used in power facilities utilizing other fuel pairs [e.g., O_{2l} + kerosene with a small amount of ionizing seeds of an alkali metal (approximately 1-2% of potassium)]. Estimates indicate that the effective conductivity of the combustion products of fuels based on O_{2l} + kerosene seeded with alkali metals is of the same order as that for the $O_{2l}+H_{2l}+Cs$ fuels [29]. This fact allows one to conclude that, in this case, the electrical power of multipolar MHDG with the same size of the MHD channel and magnetizing force of the magnet system (B~1.5T) will be close in magnitude to the respective theoretical values of N given in the table and in Fig.7. Note that in propulsion units with MHDG utilizing O_{2l} + kerosene, a superconducting version of the magnet system is preferable. Prior to starting, this system is cooled with liquid helium on the ground. The loss of liquid helium caused by

the heat flows to the cold zone of the superconducting magnet system on board the aircraft will be relatively low (less than 1 *kW/h*) in the presence of intermediate cryostatic screens cooled by liquid oxygen [4].

Table 1

Power facility parameters	Value	
I. **Propulsion unit**		
Total flow rate of the working medium G_Σ, kg/s:	200	
Flow rate of fuel H_2/oxidizer O_2 G_H/G_O, kg/s	30/170	
Pressure in the combustion chamber p_c, MPa	5	
Temperature in the combustion chamber T_c, K	3500	
Expansion ratio with respect to pressure ε	100	
Specific thrust (without MHDG) P_{sp}, m/s	4125	
Engine thrust ignoring. MHDG P_Σ, ton	82.5	
Thermal power of the propulsion unit N_Σ, MW	2000	
II. **MHD channel**		
Inlet Mach number M_{ch}	2.4	
Inlet temperature T_{ch}, K	2600	
Inlet pressure P_{ch}, MPa	0.37	
Inlet conductivity σ_{ch}, S/m	15.0	
Number of pole pairs P	3	5
Hall parameter β	0.17	0.25
Generator power N_{ch}, MW	7.0	10
Voltage U, kV	1.6	1.18
Electric current I, kA	4.45	8.47
III. **Magnet system**		
Current density J_m, MA/m^2	100	
Magnetizing force $I_c=I_w$, MA	0.75	
Number of sections P	3	5
Induction on the external radius of MHD channel B_{ch}, T	1	1.5
IV. **Weight and size of the power facility**		
Critical section radius R_{cr}, m	0.175	
Average radius of MHD channel R_{ch}, m	0.45	
Average radius of magnet system R_m, m	0.52	
Nozzle radius at the outlet R_a, m	0.65	
MHD channel length l_{ch}, m	0.6	
Magnet system length l_m, m	0.75	
Total length of the power facility (combustion chamber + nozzle) L, m	2.75	
Total weight of MHDG γ_w, kg	200	
Specific weight of MHDG γ, kg/kW	0.036	0.02
Specific thrust loss of propulsion unit + MHDG: $P_{sp\ mhdg}/P_{sp}$	0.004	0.006

At the present time MHD control possibility of supersonic boundary layer in the problems of internal and external ballistics is widely discussed. It is supposed to change pressure distribution and, consequently, balance of aerodynamics forces along surface flowing around with use of the decelerating or accelerating MHD force which able to cause a separation or reattachment of supersonic boundary layer [30]. The analysis of the turbulent boundary layer separation carried out in our paper [30] has been based on the traditional approach widely used for example in paper [31] to treat separation phenomena in conventional gasdynamics.

A positive pressure gradient in the flow leads to the flow deceleration in the inviscous core as well as in the boundary layer. Due to a difference between the core and boundary layer velocity (the boundary layer velocity is significantly lower) positive pressure gradient results in a much higher deceleration near the wall then in the flow core. Thus, the velocity profile becomes less filled and the friction tension

$$C_f = \frac{\tau_w}{\rho u_e^2}$$

at the wall decreases. In order to illustrate the above scheme generalized experimental data in terms of the friction coefficient and the velocity profile parameter n ($u/u_e=(y/\delta)^{1/n}$) as the function of normalized pressure gradient

$$G_1 = \frac{\theta_i}{\tau_w}\frac{dp}{dx}$$

are plotted in Figs.8 and 9. These values are

$$C_f = \frac{0.0128}{\mathrm{Re}_\theta^{0.25}}\frac{1}{1+0.22G_1}, \tag{19}$$

$$n = \frac{0.266\sqrt{1+G_1\,\delta_i/\theta_i}}{\sqrt{C_f}}\frac{1}{1+0.56G_1}. \tag{20}$$

where

$\theta_i = \int_0^\delta \frac{u}{u_e}(1-\frac{u}{u_e})dy$ — kinematics thickness of momentum loss;

$\mathrm{Re}_{\theta_i} = \frac{\rho u_e \theta_i}{\mu}$ — Reynolds Number based on momentum loss thickness θ_i and characteristic boundary layer temperature:

δ_l, δ — boundary layer and viscous sublayer thickness.

index «*e*» corresponds to external border of the turbulent boundary layer.

At the separation point C_f=0 and from the friction law (19) the separation criteria can be derived in the form

$$\mathrm{Re}_{\theta_i}^{0.25} \frac{\theta_i}{\rho u_e^2} \frac{dp}{dx} = 0.058, \qquad (21)$$

In Fig.10 the comparison of this criteria with experimental data from paper [3] are presented in term of value

$$\frac{\delta^{**}}{\rho_e u_e^2} \frac{dp}{dx}.$$

The flow separation under external counter pressure gradient develops through the external pressure penetration into the nozzle along the subsonic portion of the boundary layer. The gas flow deceleration caused by such a pressure gradient results in a strong growth of the boundary layer. Streamlines are declined apart the nozzle walls providing the compression in the inviscouse core flow. Intersection of the compression waves creates an oblique shock in inviscous core and the pressure growth till the atmospheric pressure that provides the external flow and boundary layer flow conjunction. The process of viscous-inviscouse interaction on the external pressure penetration length is described approximately by the separation criteria (21) and Prandtl-Mayer expression for pressure growth in a week compression wave.

$$\frac{dp}{\rho_e u_e^2} = \frac{1}{\sqrt{M_e^2 - 1}} \frac{d\delta^{**}}{dx}.$$

Then the dependencies of the critical pressure ratio p_2/p_1 and the interaction zone size l_p on flow parameters with empirical coefficients derived from experimental data comparison are as follow

$$\frac{p_2}{p_1} = 1 + 0.68 \left(\frac{\rho}{\rho_e} \right)^{0.5} \mathrm{Re}_{*\theta_i}^{-0.125} \frac{\gamma M_e^2}{(M_e^2 - 1)^{0.25}}, \qquad (22)$$

$$l_p = 19.1\theta_i \left(\frac{\rho_w}{\rho}\right)^{0.5} \mathrm{Re}_{\theta_i}^{0.125} (M_e^2 - 1)^{-0.25}. \qquad (23)$$

It was found that the above defined values for different cases of supersonic flow separation: in front of step obstacle, a wedge, under incident shock wave interacting with boundary layer and under off-design nozzle flow are practically the same. It means that the process is defined by the selfsimilarity and, consequently, flow parameters distribution in the separation point region as well as size of the latter are independent on the reason of the separation. This fact will be used to derive the separation criteria for MHD interaction case.

Despite the great practical interest the turbulent layer separation phenomena in MHD generator flows are studies insufficient up to now. For example, there are many publications on experimental results about MHD separated flow in «PAMIR» type MHDG [17,32-34] and only one paper by A.V.Gubarev [35] devoted the more or less closed theoretical model of MHD separated flow description.

MHD Separation Criteria.

Let us consider an incompressible turbulent boundary layer on a flat wall in the presence of constant mass body force. Let's assumed that the force is directed against the flow. The equations describing such a flow are as follows:

$$\frac{\partial u}{\partial x} + \frac{\partial v}{\partial y} = 0,$$

$$\rho u \frac{\partial u}{\partial x} + \rho v \frac{\partial u}{\partial y} = -\frac{dp}{dx} + \frac{\partial \tau}{\partial y} - f,$$

with traditional boundary conditions at the wall and at the core flow. Let us introduce an external force potential

$$\Phi = fx \quad ,$$

where x is a distance between leading edge of the flat and an observation point.

Then the momentum equation can be rewritten as

$$\rho u \frac{\partial u}{\partial x} + \rho v \frac{\partial u}{\partial y} = -\frac{d}{dx}(p + \Phi) + \frac{\partial \tau}{\partial y}.$$

and it is clearly seen now that the full similarity exists between the positive pressure gradient and longitudinal external body force effects. Then the separation criteria (21) can be rewritten for new conditions in the form:

$$\mathrm{Re}_\theta^{0.25}\frac{\theta_i}{\rho u_e^2}\left(\frac{dp}{dx}+f\right)=0.058.$$

In the case with no external pressure gradient the latter can be simplified to

$$\mathrm{Re}_\theta^{0.25}\frac{\theta_i}{\rho u_e^2}f=0.058.$$

This new separation criterion has been obtained under assumption of the full similarity of the pressure gradient and body force effects and, consequently, for supersonic flow supposes implicitly that the characteristics length of body force action is equal (or the same order of magnitude) as it is for the pressure gradient case, i.e. defined by formula (22). From the other hand characteristic length of the body force action is determined rather by external reasons such as, for example, a magnetic system size. Consequently, the separation criteria should be modified. In order to do this we assume here that the separation work is independent on physical reason of separation. Then

$$fl=\left(\frac{dp}{dx}\right)_{cr}l_p=\frac{p_2-p_1}{l_p}l_p=p_1\left(\frac{p_2}{p_1}-1\right)\ ,$$

and using (22) and (23), the modified criteria can be found in the following form:

$$\frac{fl}{\rho_e u_e^2}=0.684\left(\frac{\rho}{\rho_e}\right)^{0.5}\mathrm{Re}_\theta^{-0.125}(M_e^2-1)^{-0.25}\ , \tag{24}$$

where l is the characteristics length of the region where the body force acts.

At the point where $p=p_h$ the following formula is valid:

$$\frac{fl}{\rho_e u_e^2}=0.11 \tag{25}$$

here p_h — is an ambient atmospheric pressure at altitude h.

As a confirmation of the criteria obtained above the result of the experimental data on boundary layer separation published in paper [35] can be presented in the form

$$\frac{jBl}{\rho u^2}=0.1\ ,$$

that coincides practically with (25).

It was shown in numerical simulation studies [36-38] that the turbulent boundary layer separation at the electrode zone outlet happened when the integral MHD interaction parameter becomes equal

$$\frac{IB<y>}{G<u>} = 0.043 \quad . \qquad (26)$$

where $I=j<x><z>$ — total channel current.

$<y>$ — characteristics transversal size of the channel.

$G=<\rho u><y><z>$ — characteristics mass flow rate.

These expressions can be transformed to the form similar to (25)

$$\frac{fl}{\langle\rho\rangle\langle u\rangle^2} = 0.043$$

that is rather closed to the local criteria value.

Separation by induced current.

Using (6) the body force needed for separation is defined as

$$f = 0.684\left(\frac{\rho}{\rho_e}\right)^{0.5} \mathrm{Re}_{\theta}^{-0.125}(M_e^2 - 1)^{-0.25}\frac{\rho_e u_e^2}{l} \qquad (27)$$

Taking l=0.5m as a minimal linear scale of an external magnetic system one can find that

$$f=0.370\ \mathrm{MN/m^3}. \qquad (28)$$

that is very closed to the estimation presented in paper [39].

Electromagnetic force is $\mathbf{j}\times\mathbf{B}$ and can be estimated for the induced current case as $f\approx\sigma u B^2$. where σ is electrical conductivity. Thus the needed magnetic induction is

$$B = \sqrt{\frac{f}{\sigma u}} \qquad (29)$$

For rough estimation we use two different semiempirical formula for electrical conductivity presented in Figs.11-12: the first case corresponds to «optimistic» evolution of conductivity of PAMIR working fluid seeded with *Cs*: conductivity was calculated with the formula

$$\sigma = \sigma_{\infty}\left(\frac{T}{T_{\infty}}\right)^{3/4}\left(\frac{p}{p_{\infty}}\right)^{-1/2}\exp\left(-W\left(\frac{1}{T}-\frac{1}{T_{\infty}}\right)\right) \qquad (30)$$

where σ_*=43.3Sm/m at T_*=2370K and p_*=0.185MPa, W=22557K; the second case corresponds to the CO_2 seeded with Cs used in MHD generator experiments on the facility with shock tube [40]; the conductivity was calculated with the formula

$$\sigma = \alpha T^{3/2} p^{-1/2} \exp(-W/T) \tag{31}$$

where α=5.75×10^{-4} is the mass fraction of Cs vapor in the working fluid.

For the first case the magnetic induction level providing the boundary layer separation is found as high as B=8.4T that seems to be far from the thecnically realized values for a transportable device. Thus it can be calculated that the controlled boundary layer separation in the typical nozzle flow is hardly be provided with the induced current only because of relatively low temperature (and conductivity) in the flow.

Separation by externally applied current.

From the expression (28) one can define that the value of current density is to be not lower than j≈2.3×10^{5}A/m^2 for the case of the external magnetic induction is equal to 2T.

The power supply needed is estimated with energy equation in the form

$$\rho u c_p \frac{dT}{dx} = \frac{j^2}{\sigma},$$

or, in an integral form

$$\int_{T_1}^{T_2} \sigma(T)\,dT = \int_0^l \frac{j^2}{\rho u c_p}\,dx.$$

Using some linearization procedure described in Ref. [30], a total heat power delivered in the current affected region is

$$Q = 2\pi r\delta \int_0^l j^2/\sigma\,dx = 2\pi r\delta \rho u c_p (T_2 - T_1).$$

For the minimum current density estimated earlier in this section j≈2.3×10^{5}A/m^2 the total head power is about Q=26MW. This value is approximately equal to 5% of the typical rocket engine power under conditions considered in [30].

CONCLUSION

(1) The power facility considered with a built-in multipolar MHD generator makes it possible to obtain electric power using the MHD conversion of a part of the gas flow energy in the peripheral zone of the rocket engine jets.

(2) The analysis of volumetric MHD effects and output characteristics of a multipolar MHDG with electrode modules of different design has revealed that the theoretical dependences are in satisfactory agreement with the experimental data obtained in the plasma model of a multipolar MHD channel.

(3) An optional design of a power facility has been developed, in which a multipolar MHDG is built in the nozzle. The MHD generator utilizes the products of combustion of cryogenic fuel $H_{2l}+O_{2l}$, seeded with cesium. It is demonstrated that such a facility can provide the power output of about 10MW. The loss of specific thrust of the propulsion unit is relatively low (less than 1 %).

(4) The proposed version of a power facility with a built-in multipolar MHDG may show promise when the engine utilizes other fuel vapours (e.g., oxygen and is kerosene seeded with potassium).

(5) A simplified model and corresponding estimation procedure for MHD separation of turbulent boundary layer has been proposed.

(6) It was found that for typical conditions of rocket engine nozzle flow an induced current separation control is hardly reachable due to low boundary layer temperature and practical limitations for magnetic induction level.

(7) An externally applied electrical power can provide the controlling boundary separation in a nozzle flow.

REFERENCES

1. ***Spitzer, C.R.***, A New Direction in Energy Conversion. The All-Electric Aircraft. *Proc. 20th Intersoc. Energy Conversion Eng. Conf., New York, 1986, V.1, p.388.*

2. ***Spitzer, C.R.***, *IEEE Trans. Aerosp. Electron. Syst., 1984, No. 3 (20), p.261.*

3. ***Secunda, R.R.***, *AIAA Paper, 1972, No. 1056.*

4. ***Kovalev, L.K., But, D.A., Poltavets, V.N.***, and ***Koneev, S.-M.A.***, Analysis of Thermal Processes in Electrode Walls and Their Influence on the Operation of MHD Installations. *Proc. 6th Int. Conf on MHD Electrical Power Generation, USA, 1975.*

5. ***Carabetta, R.A., Chambers, H.F., Staats, Jr., G.F.***, and ***Owens, W.R.***, *An Overview of DOE and SDIO MHD Program Activities at PETS 26th Aerospace Sciences Meet., Jan. 11-14, 1989, Reno, Nevada.*

6. ***Kovalev, L.K., Larionov, A.E., Poltavets, V.N.***, and ***Kovalev, K.L.***, Theoretical and Experimental Studies of Faraday Multi-Pole MHD Generators. *Proc. the 11th Int. Conf. on MHD Electrical Power Generation, China, 1992.*

7. ***K.L.Kovalev*** and ***T.A.Markina***. Power Facility with a Built-in Multipolar MHD Generator. *High Temperature, V.33, No. 3, 1995, pp. 460 - 468.* (Translated from Teplofizika Vysokich Temperatur V.33, No. 3, 1995, pp. 463 - 472.)

8. ***Marston Charias, H.***, *AIAA J., 1987, V.4, No. 11.*

9. ***Moder, J.P., Blandio, J.S., Frazier, S.R.***, and ***Rosa, R.J.***, *AIAA Paper, No. 1816, 1987.*

10. ***K.L.Kovalev, T.A.Markina, Poltavets, V.N.***, Energosilovye ustanovki s vstroennym MGD generatorom (Power Facility with Build-in MHD Generator). *Proceeding of Moscow Conference on Prospective R&D, 1993.*

11. ***V.A.Bityurin, V.A.Zeigarnik, A.L.Kuranov***. On a Perspective of MHD Technology in Aerospace Applications. *AIAA Paper 96-2355, 1996.*

12. ***V.A.Bityurin, A.M.Gubertov, V.A.Ivanov, M.L.Kuranov, V.I.Okunev***. MHD Control Estimation of Supersonic Boundary Layer. *Twelfth International Conference on Magnetohydrodynamic Electrical Power Generation, Yokohama, Japan, October 15-18, 1996, v.12 p.618.*

13. ***Goldin A.Ya., Ievlev V.M., Paveliev A.A, Prishletzov A.B.,*** High Temperature Gas-Phase Nuclear Reactor – Perspective for Space Pocket Engine and Power Systems. *Proc. of International Conf. on Nuclear Power for Space. Obninsk. 1990. USSR.*

14. ***Koroteev A.S., Semenov V.F., et al,*** Emery and Thrust Providing System for Manned Mission to Mars. *Proc. of International Conf. on Nuclear Power for Space. Obninsk. 1990. USSR.*

15. ***Kovalev, L.K., Koneev, S.-M.A., Larionov, A.E., et al,*** Raschetno-Teoreticheskie issledovanija energosilovoy ustanovki (Parametric Studies of a Power Generating Facility). *Report No. 3/149. 1991. MAI. Moscow* (in Russian).

16. ***Glinik R.A., et al,*** Yadernaja energodvigatelnaja ustanovka na osnove vysokotemperaturnogo gasofasnogo reaktora dla pilotiruemoy ekspeditzii k Marsu (Nuclear Power/Thrust unit based on a High Temperature Gas-Phase Reactor). *Kosmicheskaja Technica (Astronavtic Technology). NIITP. No.1 (134). 1992. p.75-92* (in Russian).

17. ***Breev, V.V., Gubarev, A.V.,*** and ***Panchenko, VR,*** Sverkhzvukovye MGD Generatory (Supersonic MHD Generators). *Moscow: Energoizdat. 1988* (in Russian).

18. ***Aitov, N.L., Zeigarnik, V.A., Rikman, V.Yu., Koneev, S.-M.A., Kovalev, L.K., Larionov, A.E.,*** and ***Poltavets, V.N.,*** An Experimental Studies with Disk MHD Channels on Argon Plasma. *Proc. 32nd SEAM. USA. 1994.*

19. ***L.K.Kovalev, K.L.Kovalev.*** Faraday DC and AC Multipole MHD generators. *Electtrichestvo (Electricity). No.7. 1991. p.26.* (In Russian).

20. ***Kutateladze, S.S.*** and *Leont'ev, A.I.,* Teplo-massoobmen i Trenie v Turbulentnom Pogranichnom Sloe (Heat and Mass Transfer and Friction in Turbulent Boundary Layer). *Moscow: Energiya. 1972* (In Russian).

21. ***Krasnov, N.F.,*** Aerodinamika (Aerodynamics). *Moscow: Vysshaya Shkola. 1980. V.2* (In Russian).

22. ***Kovalev, L.K., Koneev, S.-M.A., Larionov, A.E.,*** and ***Tsar'kov, V.D.,*** *Magnitnaya Gidrodinamica. 1990. No. 4.*

23. ***But, D.A., Glinik, R.A., Keilin, YE., et al,*** *Voprosy Nauki i Techniki. Seria Yaderny Syntes. 1982. No. 2 (10). p.45* (in Russian).

24. ***Abramovitch G.N.*** Applied Gasdynamics. *Mir. Moscow. 1976. p.752* (in Russian).

25. ***Bout, D.A., Kovalev, L.K.,*** and ***Larionoff, A.E.,*** Stressed Deformed State of Superconducting Windings and Ring Girders, *Proc. 10th Int. Conf on MHD Electrical Power Generation, Tiruchirappalli, India, 1989, V.1, p. 6118.*

26. Termodinamicheskie i Teplofizicheskie Svoistva Produktov Sgoraniya (Thermodynamic and Thermal Properties of Combustion Products), ***Glushko, V.R,*** *Ed., Moscow, VMTI, 1972, V. 2.*

27. ***Dudko, D.Ya., Emets, Yu.R,*** and ***Repa, I.I.,*** *Teplofiz. Vys. Temp., 1981, V.19, No. 4, p.697 (see also High Temperatures, AIPh).*

28. ***Kovalev, L.K., Nikitin, Yu.M., Nikitina, I.A.,*** and ***Tyutin, V.K.,*** *Teplofiz. Vys. Temp., 1975, V.13, No. 3, p. 605 (see also High Temperatures, AIPh).*

29. ***Nedospasov, A.V., Poberezhskii, L.P.,*** and ***Chemov, Yu.G.,*** Sostav i Svoistva Rabochikh Tel MGD Generatorov Otkrytogo Tipa (Composition and Properties of Working Media of Open-Cycle MHD Generators), *Moscow: Nauka, 1977* (in Russian).

30. ***Ivanov V.A.*** et.al. The Development of a Method of the MHD Separation Flow Calculation, *Tech. Report, 95/7, IVTAN-ANRA, Moscow, 1995, 42p* (in Russian).

31. ***Ivanov V.A.,*** The Method of the Flow and Head Transfer Calculation in a Nozzle under Off-Design Mode, *PhD Thesis, MPTI-NIITP, Moscow, 1985* (In Russian).

32. ***Aitov N.L., Zeigarnik V.A., Kulkov V.V., Isaev Yu.I., Matsenko A.B., Novikov V.A., Okunev V.I., Revtov A.N., Rikman V.Yu., Trapeznikov Yu.A., Turovets V.L.*** MHD Complex Test Bench "Pamir-2F". Capability Description. First Results, *10th International Conference on Magnetohydrodynamic Electrical Power Generation, V.4, pp.304-305.*

33. ***Dogadaev R.V., Panchenko V.P., Treiger, Ye.M., Yakushev A.A., Vengerski V.V., Belokon V.V., Okunev V.I., Ralchenko M.I.*** The Pulsed Supersonic MHD Generator with Enhached Energy Characteristics, *10th International Conference on Magneto-hydrodynamic Electrical Power Generation, V.1, pp.VII.1-VII.9.*

34. ***Bukhteyev L.A., Dogadayev R.V., Panchenko V.P., Yakushev A.A.*** Experimental end Numerical Researches of the Pulsed Solid Propellant Diagonal Type MHD Generator "Pamir-06", *Proceedings of the 33rd Sym-posium on Engineering Aspects of Mag-netohydrodynamics, Tennessee, USA, June 13-15, 1995, pp. IV.10.1-IV.10.11.*

35. ***Gubarev A.V., Tynnikov Yu.G.*** Studies of Flow in MHD Generator with Strong Deceleration. In: *Proc. of 8th Intt.Conf.. on MHD El.. Power Generation. Moscow. 1982. V.5. p.85.*

36. ***Ivanov V.A.*** Calculation of Electrical Curent in Faraday MHD Generator under Strong MHD Interaction. *High Temperature. 1992. V.30. No.4. p.822-829.*

37. ***Ivanov V.A.*** A Influence of a Transfer Flow Non-Uniformity on Boundary Layers Development in Faraday MHD Generator. *High Temperature. 1993. V.31. No.1. p.129-133.*

38. ***Ivanov V.A.*** A Method for Calculating a MHD Flow with Boundary Layer Separation. *High Temperature. 1994. V.32. No.6. p.909-919.*

39. ***Gubertov A..M.*** et al.. Development of the Calculation Method of the Heattransfer and Heatinsulation in an MHD Generator. *Tech.Report. 1911. 1994. NIITP. Moscow* (in Russian).

40. ***Bityurin V.A., Ivanov V.A., Veefkind A.*** An Investigation of the Evolution of a Curren-Carrying Plasma Clot and Pecularities of Flow in an Experimental MHD Generator with a Shock Tube. *High Temperature. V.33. No.5. 1995. pp776-788.*

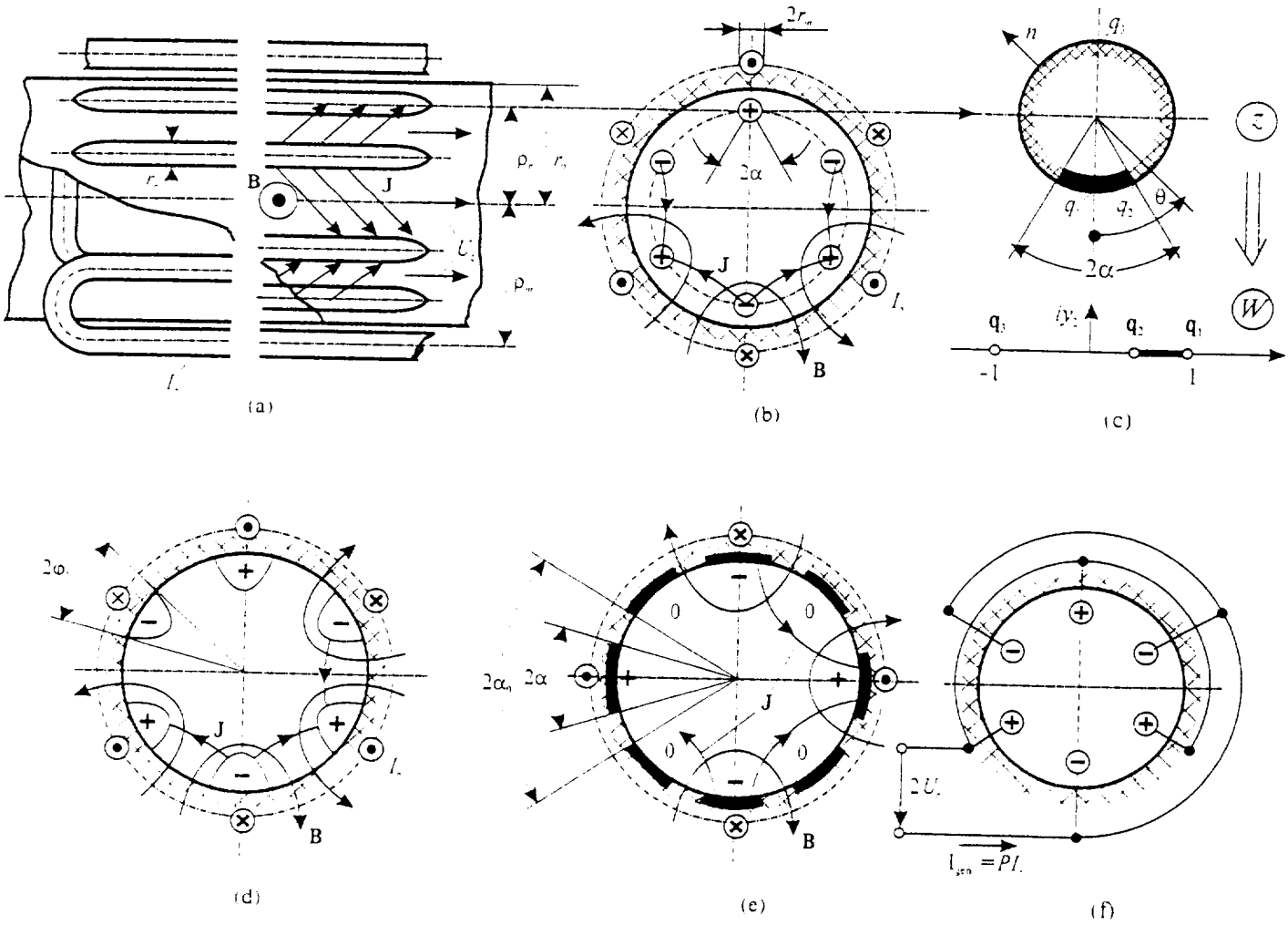

Fig.1. Multipolar MHDG schemes..

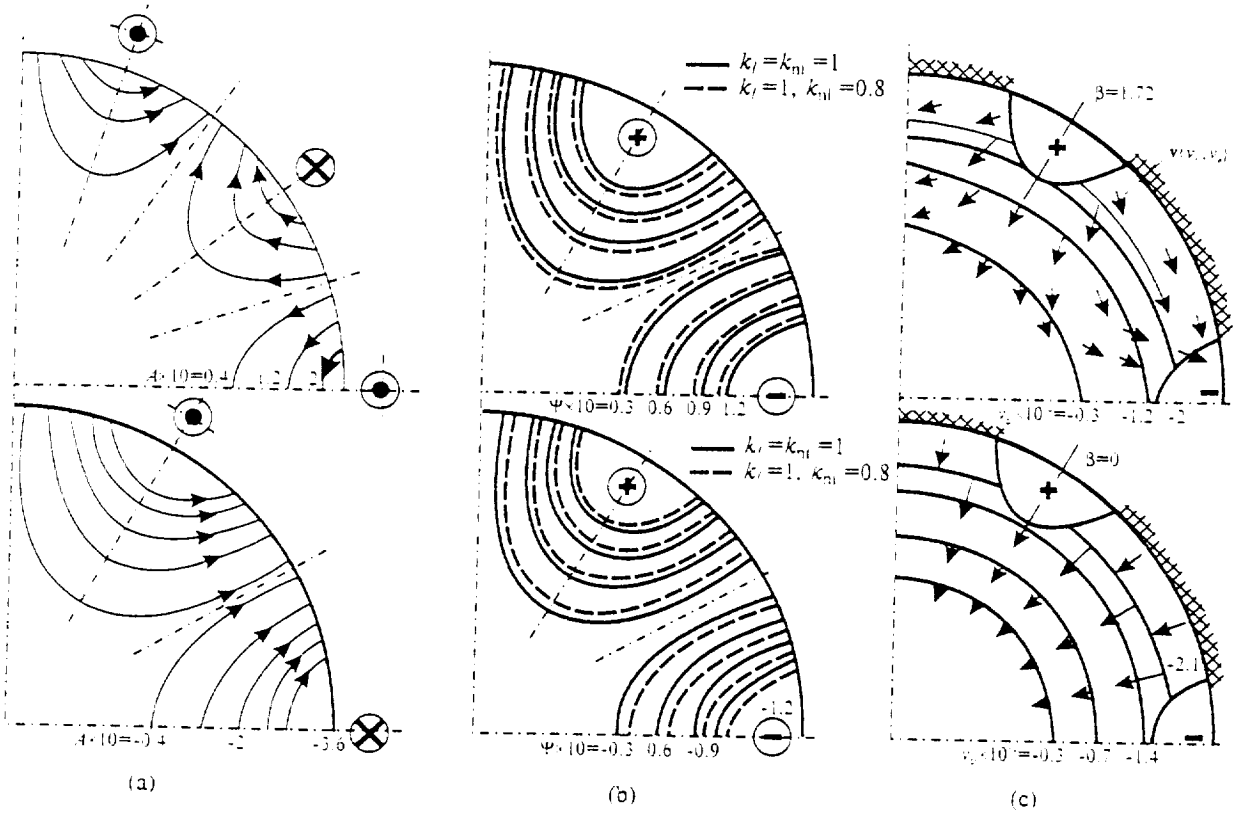

Fig.2. Distributions, over the channel section, (a) of the magnetic flux function A, (b) of the current density potential Ψ and (c) of the velocity disturbances $\mathbf{v}\{v_r, v_\theta, v_z\}$.

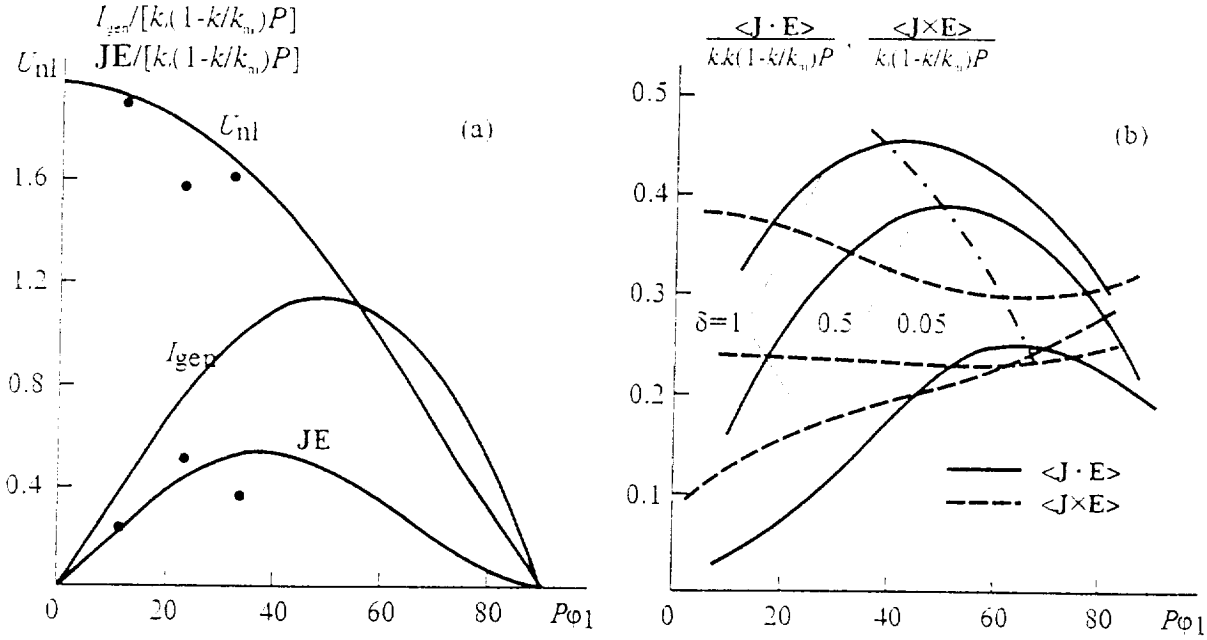

Fig. 3. Dependences of the dimensionless averaged quantities $<J \cdot E>$, $<J \times B>$ of the short-circuit current I_{sc} and the no-load voltage U_{nl} on the relative size of the electrode modules in MHD channels with (a) U-shaped electrodes and (b) segmented electrodes.

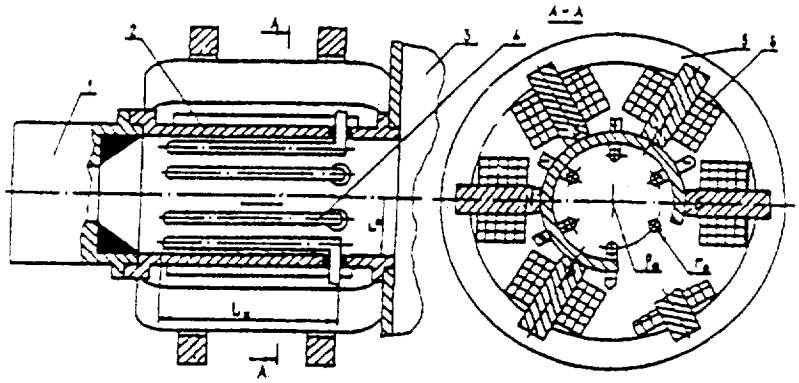

Fig.4. Experimental multipole MHD channel.

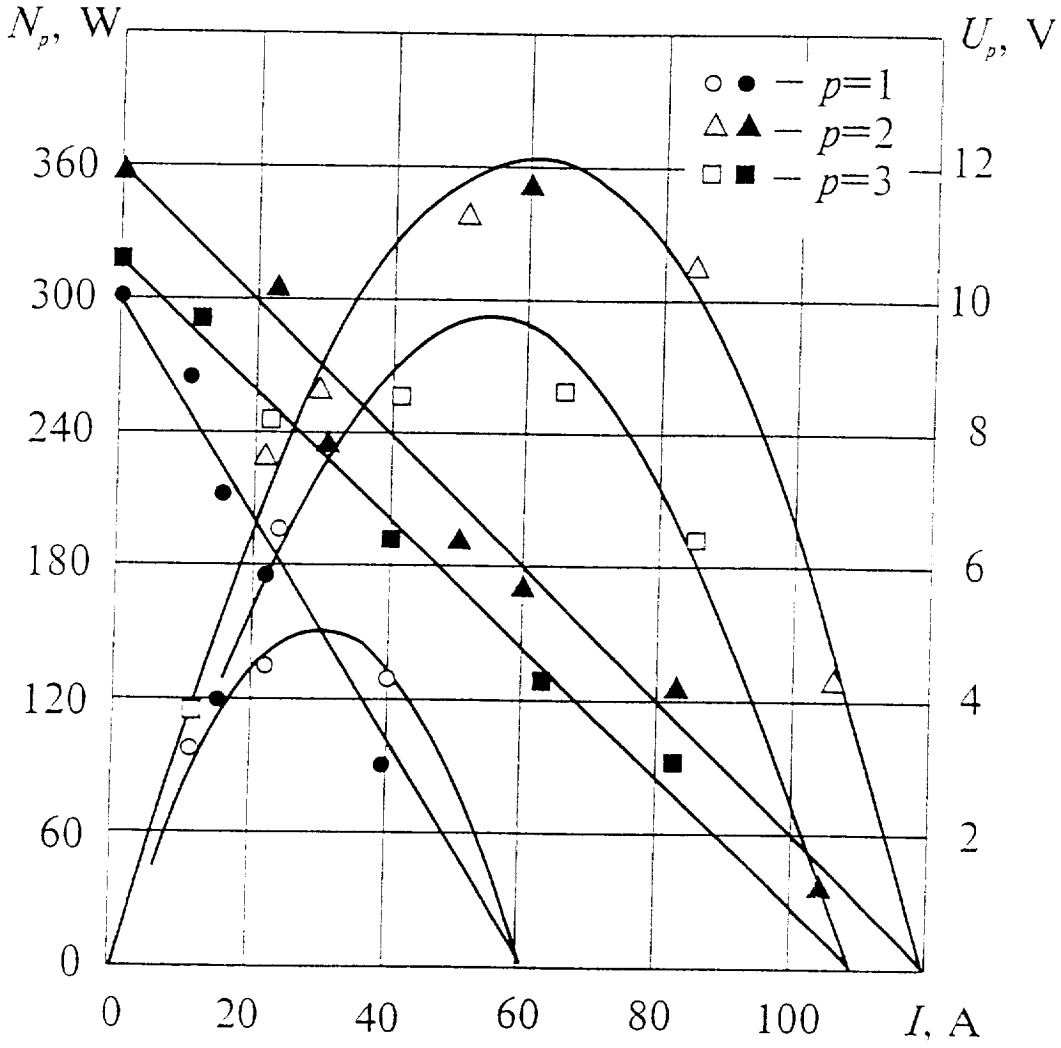

Fig.5. Experimental voltage-current $U(I)$ and power $N(I)$ characteristic.

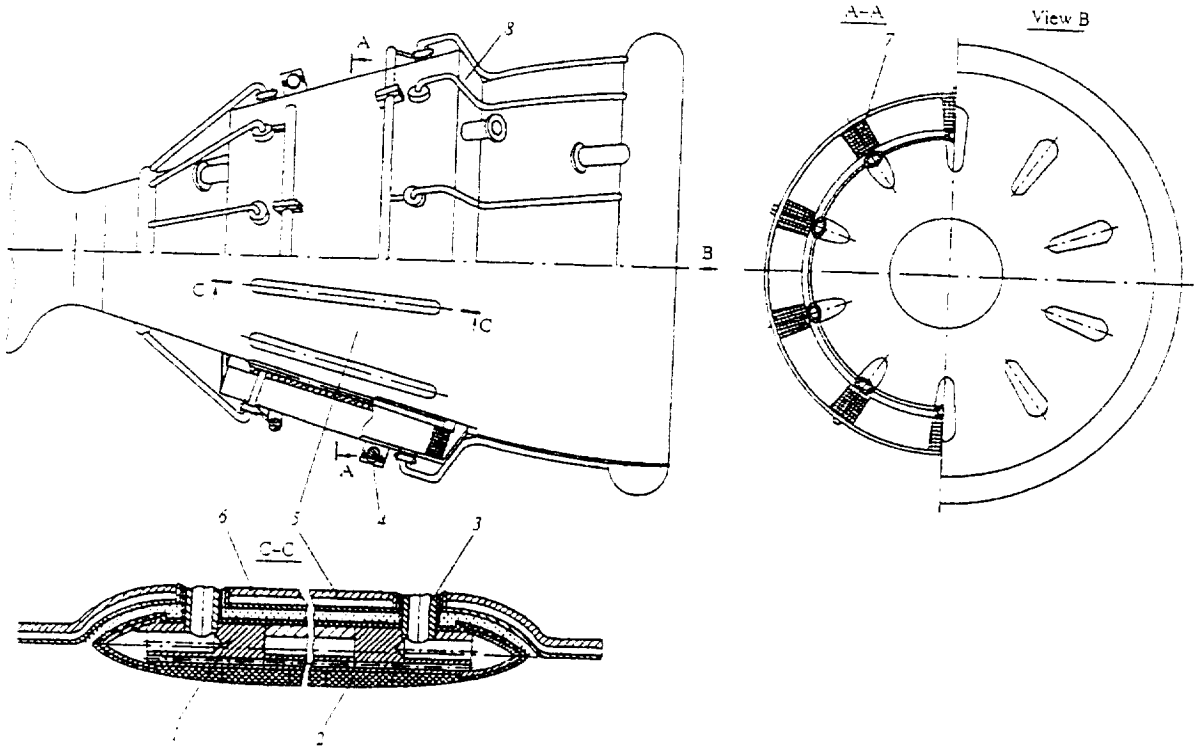

Fig.6. Design scheme of the power facility with a built-in multipolar MHDG.

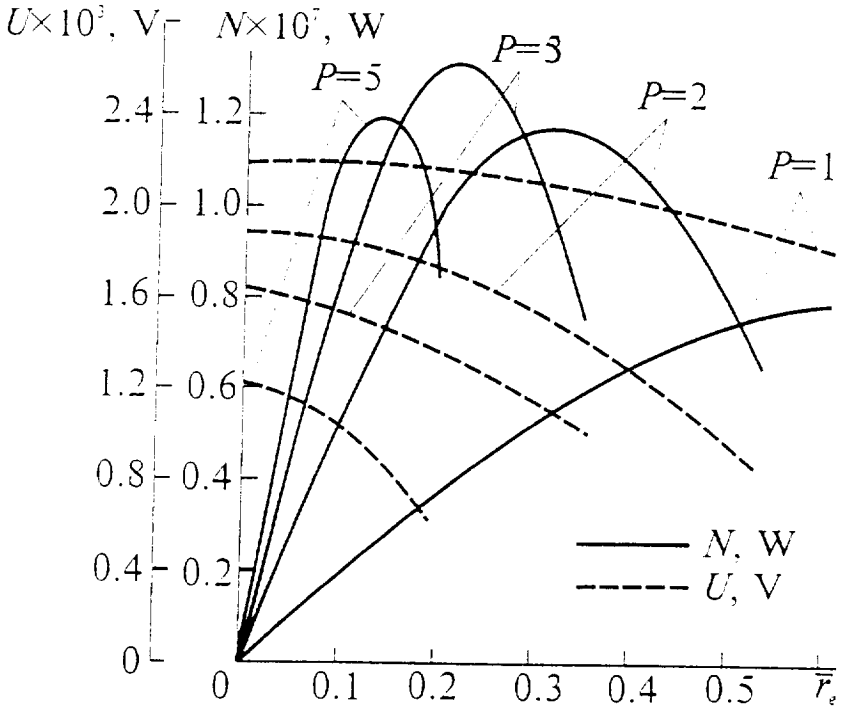

Fig.7. The power and voltage of the muldpolar MHDG as functions of the size of the electrode modules $r_e=R_{CH}$ and number of pairs P.

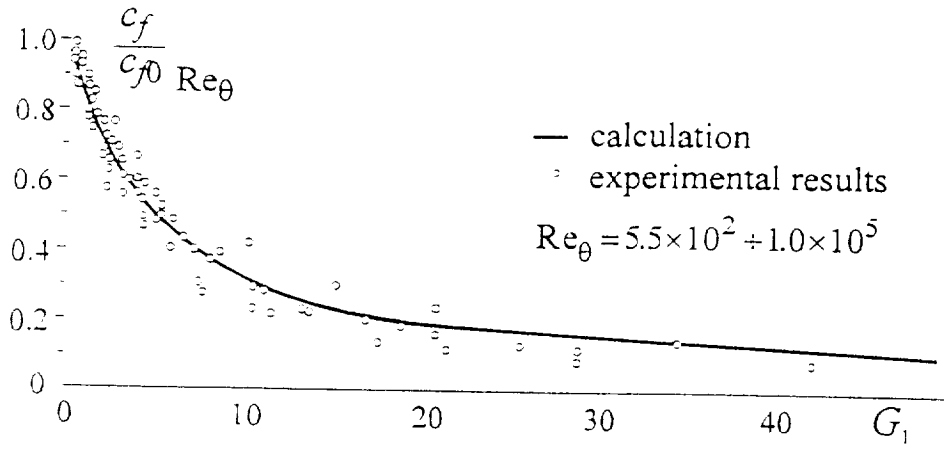

Fig.8. Relative friction coefficient against pressure gradient parameter G_1 (see text for more explanation).

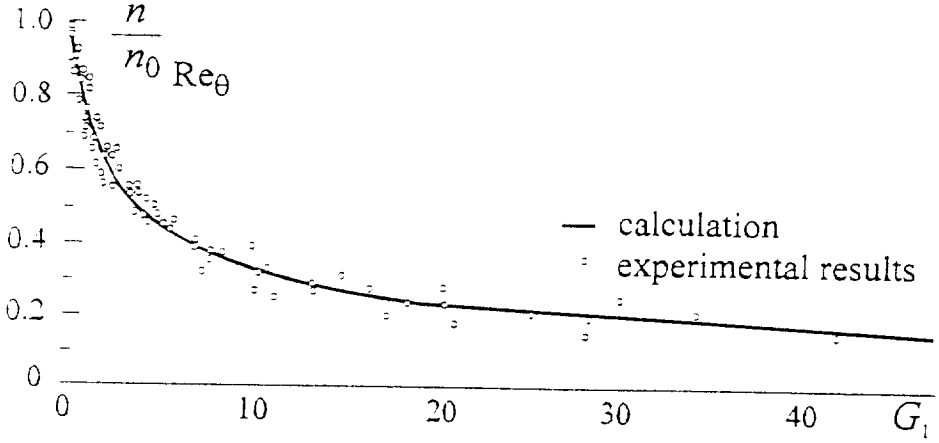

Fig.9. Relative value of the parameter n in velocity profile power low against pressure gradient parameter G_1 (see text for more explanation).

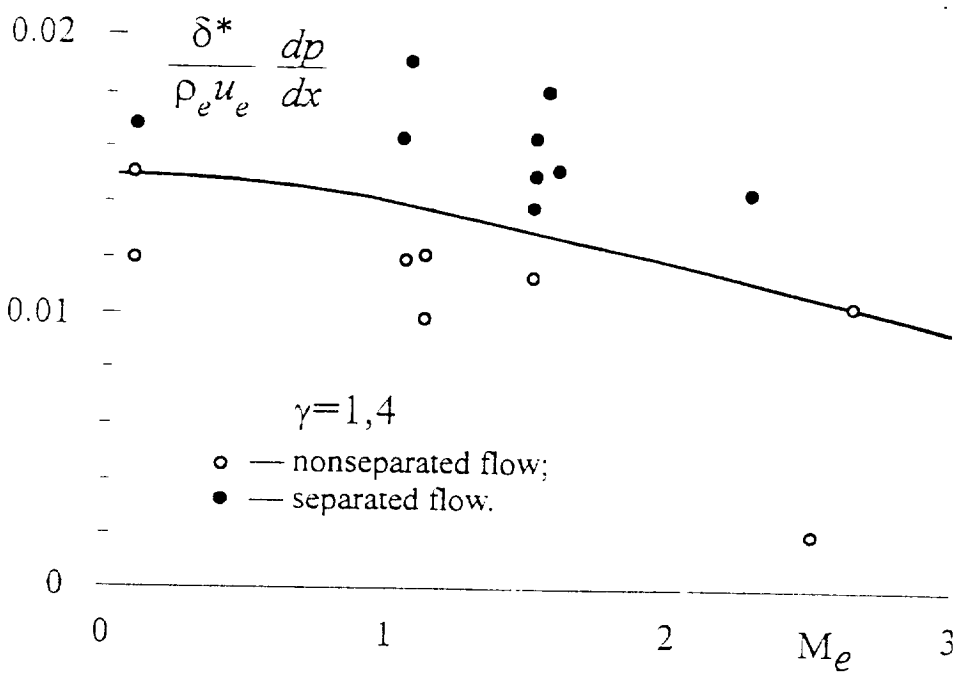

Fig.10. Separation criteria vs Mach number.

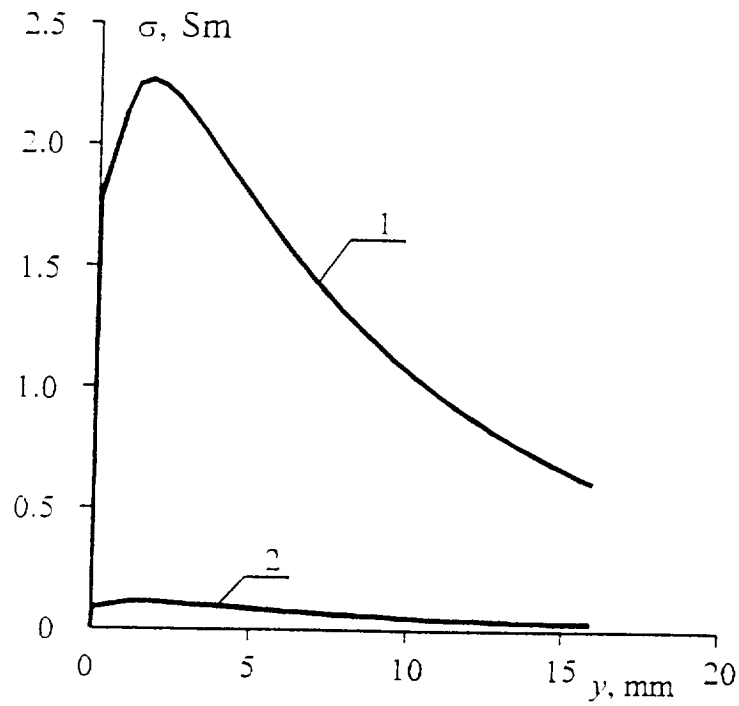

Fig.11. Conductivity profile across a boundary layer.
1 – MHD Generator PAMIR conditions.
2 – Combustion products of $CO+O_2$ Cs seed.

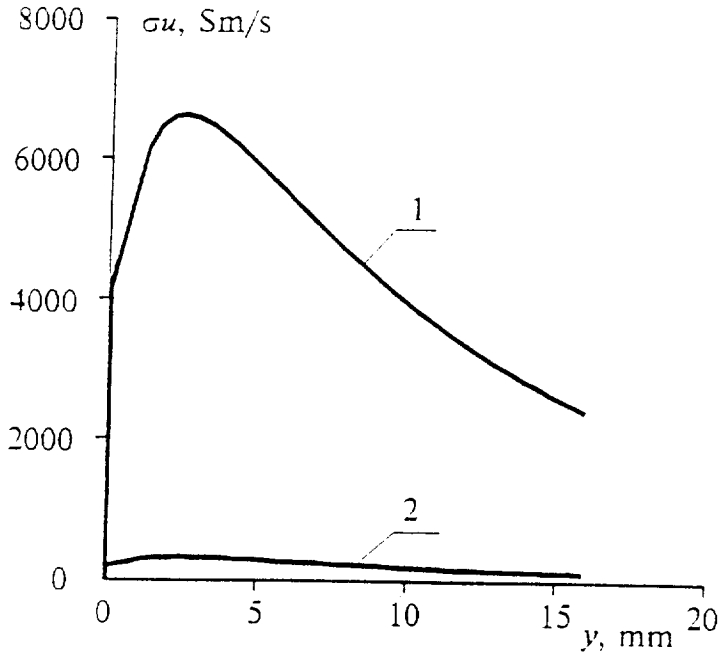

Fig.12. Effective electromagnetic force profile across a boundary layer.
1 – MHD Generator PAMIR conditions.
2 – Combustion products of $CO+O_2$ Cs seed.